minerals

Review

Paleo-Tethyan Ocean Evolution and Indosinian Orogenesis in the East Kunlun Orogen, Northern Tibetan Plateau

Ruibao Li [1,*], Xianzhi Pei [1,*], Zuochen Li [1], Lei Pei [1], Guochao Chen [1], Zhanqing Liu [2], Youxin Chen [1], Chengjun Liu [1], Meng Wang [1] and Min Zhang [1]

[1] School of Earth Science and Resources, Chang'an University, Xi'an 710054, China
[2] School of Earth Sciences, Guilin University of Technology, Guilin 541006, China
* Correspondence: liruibao0971@163.com (R.L.); peixzh@sina.com (X.P.)

Abstract: The East Kunlun Orogen on the northern margin of the Tethyan orogenic system records a history of Gondwana dispersal and Laurasian accretion. Uncertainties remain regarding the detailed histories of northern branches of the Paleo-Tethys Ocean in East Kunlun Orogen (Buqingshan Ocean). Based on a synthesis of sedimentary, structural, lithological, geochemical, and geochronological data from the East Kunlun Orogen and adjacent regions, this paper discusses the spreading and northward consumption of the Paleo-Tethys Ocean during Late Paleozoic–Early Mesozoic times. The main evolutionary stages are: (1) during Carboniferous to Middle Permian, the Paleo-Tethys Ocean (Buqingshan Ocean) was in an ocean spreading stage, as suggested by the occurrence of Carboniferous MORB-, and OIB-type oceanic units and Carboniferous to Middle Permian Passive continental margin deposits; (2) the Buqingshan Ocean subducted northward beneath the East Kunlun Terrane, leading to the development of a large continental magmatic arc (Burhan Budai arc) and forearc basin between ~270–240 Ma; (3) during the late Middle Triassic to early Late Triassic (ca. 240–230 Ma), the Qiangtang terrane collided with the East Kunlun–Qaidam terranes, leading to the final closure of the Buqingshan Ocean and occurrences of minor collision-type magmatism and potentially inception of the Bayan Har foreland basin; (4) finally, the East Kunlun Orogen evolved into a post-collisional stage and produced major magmatic flare-ups and polymetallic mineral deposits between Late Triassic to Early Jurassic (ca. 230–200 Ma), which is possibly related to asthenospheric mantle upwelling induced by delamination of thickened continental lithosphere and partial melting of the lower crust. In this paper, we propose that the Wilson cycle-like processes controlled the Late Paleozoic–Early Triassic tectonic evolution of East Kunlun, which provides significant implications for the evolution of the Paleo-Tethys Ocean.

Keywords: paleo-tethys; kunlun; forearc basin; accretionary complex; Indosinian; magmatic arc; ophiolite; granites; oceanic island basalts

Citation: Li, R.; Pei, X.; Li, Z.; Pei, L.; Chen, G.; Liu, Z.; Chen, Y.; Liu, C.; Wang, M.; Zhang, M. Paleo-Tethyan Ocean Evolution and Indosinian Orogenesis in the East Kunlun Orogen, Northern Tibetan Plateau. *Minerals* **2022**, *12*, 1590. https://doi.org/10.3390/min12121590

Academic Editor: Manuel Francisco Pereira

Received: 30 October 2022
Accepted: 6 December 2022
Published: 11 December 2022

1. Introduction

The East Kunlun Orogen (EKO), stretching more than 1000 km W-E, is located along the northern margin of the Tibet–Qinghai Plateau in Western China [1–15]. As early as the late 20th century, some pioneering explorations (e.g., Sino-French traverse) have been made in the Kunlun ranges, which established the preliminary tectonic framework of the Kunlun [1,16,17]. Since the 21st century, much work has been conducted and further suggested that EKO involves the tectonic evolution of the Proto-Tethys Ocean during Neoproterozoic to Early Paleozoic and the Paleo-Tethys Ocean during Late Paleozoic–Early Mesozoic time [12,18–23]. The Proto-Tethys Ocean was closely related to the breakup of the supercontinent Rodinia and likely closed in the Silurian time based on occurrences of high-pressure (HP) to ultrahigh-pressure (UHP) metamorphic rocks, A-type granites, Cu-Ni-Co sulfide deposits, and foreland basins [24–31]. Subsequently, the Paleo-Tethys Ocean gradually opened in Kunlun and Qinling area during Middle Devonian [32]

The northernmost branch of the Paleo-Tethys Ocean in China is locally referred to as the Buqingshan Ocean in the EKO and can be linked to the Mianlue Ocean further to the east in the Qinling region, and the Kangxiwa Ocean to the west in West Kunlun (Figure 1b) [33–37]. Previous researchers have reconstructed the general tectonic framework and evolution history of this ocean from Late Paleozoic to the Mesozoic. However, some debate continues regarding the details of its evolutionary history. Controversies mainly include: (1) when the ocean began to subduct and when it closed; (2) spatiotemporal relationships amongst Buqingshan tectonic complexes, Early–Middle Triassic strata, and multiple magmatic episodes; (3) when the Qiangtang terrane collided with the consolidated Kunlun–Qaidam terrane and then docked to the southern margin of Laurasia; and (4) when these blocks assembled and formed the East Asia continent. Some researchers argue that the Paleo-Tethys Ocean closed in the Late Permian, and then entered a syn-collisional stage in the Early Triassic and a post-collisional stage in the Middle–Late Triassic [38–42]. Others suggest that the Paleo-Tethys Ocean closed in the late Middle Triassic (Ladinian), subsequently evolving to a post-collisional stage in the Late Triassic based on the Late Permian–Early Triassic arc granites and Late Triassic collision-type magmatism [22,34,43–50]. Recently, some new data suggested that Permian to Triassic magmatism in the EKO occurred in an island arc setting, which indicates continuous northward subduction of the Paleo-Tethys Ocean until the Late Triassic [12,13,51]. Most previous research has focused on the geochronology and geochemistry of magmatic rocks. The tectonic affinities of multiple magmatic phases, basin analysis of Late Paleozoic–Triassic strata, and overall spatiotemporal relationships still await detailed investigation.

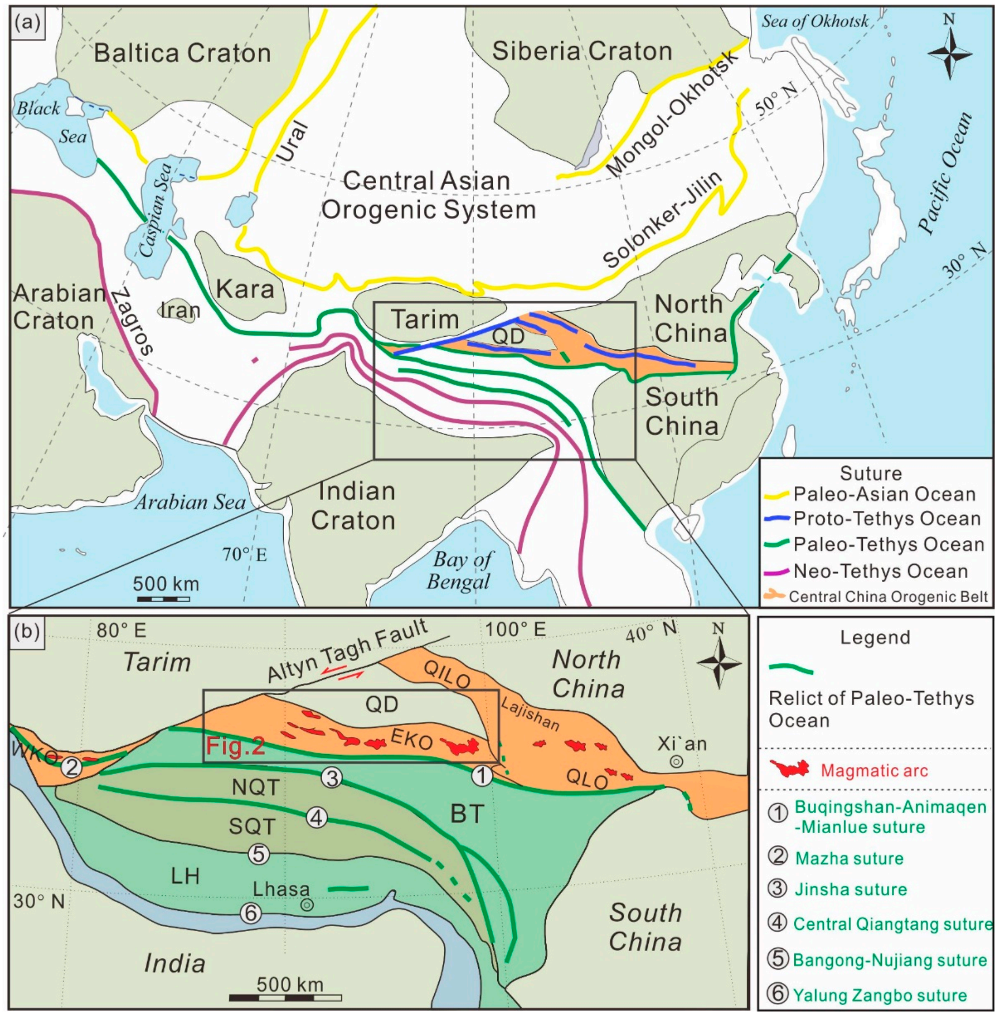

Figure 1. (a) Simplified tectonic map of Asia showing cratons and sutures (modified from Zuza and

Yin [52]), and (**b**) tectonic framework of the Northern Tibetan Plateau (modified from Roger et al. and Xu et al. [11,51]). Kara—Karakum; NQT—North Qiangtang terrane; SQT—South Qiangtang terrane; QD—Qaidam; BT—Bayan Har terrane; LH—Lhasa terrane; QLO—Qinling Orogen; QILO—Qilian Orogen; EKO—East Kunlun Orogen; WKO—West Kunlun Orogen.

In this paper, we integrate new sedimentary and detrital zircon geochronological data from EKO with available magmatic, sedimentary, geochemical, and structural records relevant to the Late Paleozoic–Mesozoic evolution of the EKO. Based on these data, we aim to provide important insights into the development of the northern branch of the Paleo-Tethys Ocean and reconstruct the paleogeography of the Northern Paleo-Tethys Ocean in EKO.

2. Regional Geology

The EKO is located in the northern part of the Tibet–Qinghai Plateau, China (Figure 1a,b). It consists, from north to south, of the North Kunlun terrane (NKT), the South Kunlun terrane (SKT) and the Bayan Har terrane (BT) [14], which are separated by the Central Fault of East Kunlun and the Buqingshan accretionary complex (Buqingshan AC), respectively (Figure 2a,b).

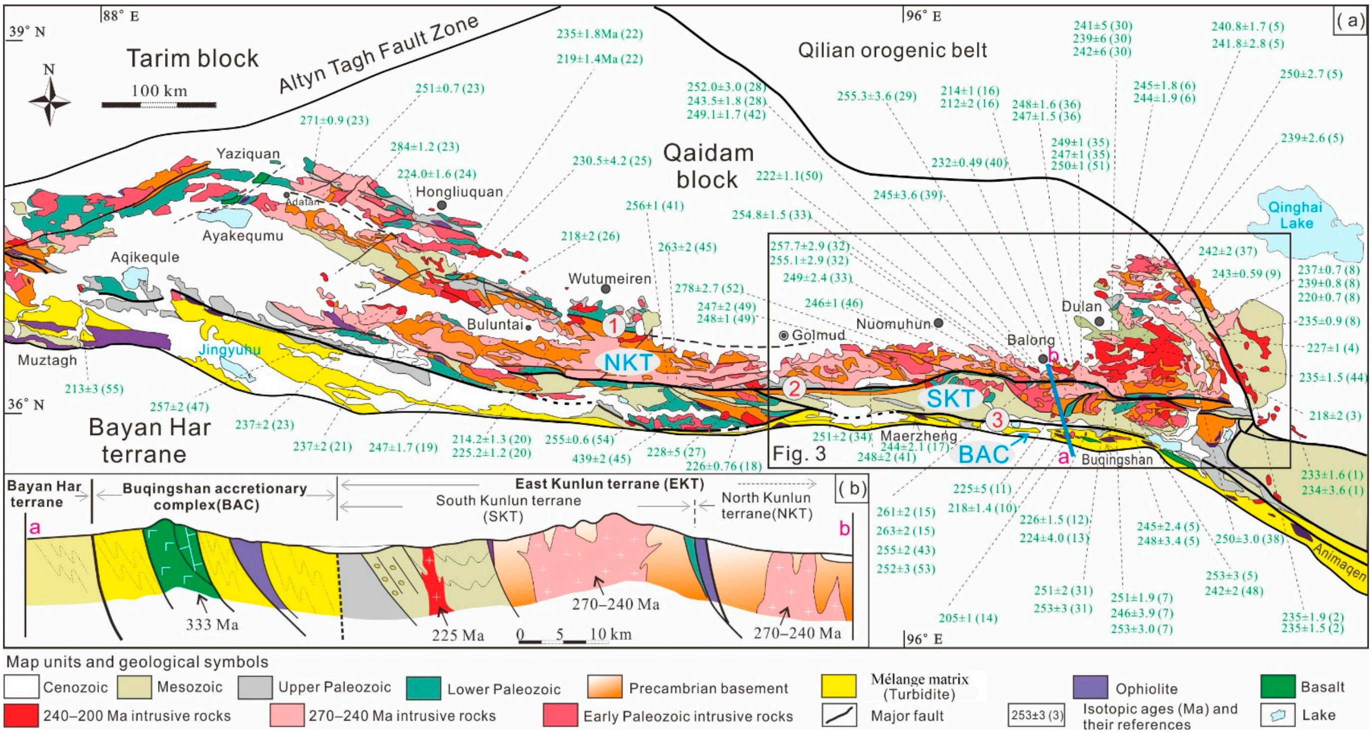

Figure 2. (**a**) Tectono-magmatic sketch map of the East Kunlun Orogen showing rock associations; (**b**) integrated cross section showing tectonic units and rock associations. The location of Figure 3 is outlined. ①—Qimatag–Xiangride fault; ②—Central fault of East Kunlun; ③—South fault of East Kunlun; NKT—North Kunlun terrane; SKT—South Kunlun terrane; BAC—Buqingshan accretionary complex. Data sources: 1—Zhang et al. [53]; 2—Xiong et al. [54]; 3—Zhang et al. [55]; 4—Li et al. [56]; 5—Chen et al. [57]; 6—Li et al. [58]; 7—Chen et al. [45]; 8—Shao et al. [59]; 9—Li et al. [60]; 10—Chen et al. [44]; 11—Chen et al. [44]; 12—Li et al. [61]; 13—Liu et al. [62]; 14—Li et al. [63]; 15—Xiong FH et al. [64]; 16—Ding et al. [65]; 17—Liu et al. [66]; 18—Deng et al. [67]; 19—Wei et al. [68]; 20—Chang et al. [69]; 21—Wang et al. [70]; 22—Feng et al. [71]; 23—Wang et al. [72]; 24—Li et al. [73]; 25—Xi et al. [74]; 26—Wu et al. [75]; 27—Wu et al. [20]; 28—Zhang [76]; 29—Sun et al. [77]; 30—Liu et al. [78]; 31—Chen et al. [46]; 32—Zhang [76]; 33—Li et al. [79]; 34—Xiong et al. [64]; 35—Li et al. [49];

36—Li et al. [50]; 37—Zhao et al. [80]; 38—Kong et al. [81]; 39—Zhang et al. [82]; 40—Chen et al. [46]; 41—Xue et al. [83]; 42—Xiong et al. [27,28]; 43—Xiong et al. [84]; 44—Xin et al. [85]; 45—Wu et al. [20]; 46—Song et al. [86]; 47—Yao et al. [87]; 48—Chen et al. [88]; 49—Ding et al. [89]; 50—Xia et al. [90]; 51—Huang et al. [40]; 52—Liu et al. [18]; 53—Zhang et al. [76]; 54—Shi et al. [91]; 55—Yuan et al. [92].

2.1. North Kunlun Terrane

The NKT features exposures of Precambrian basement and Paleozoic metamorphic rocks (Figures 2a, 3 and 4) intruded by Paleozoic–Mesozoic granitoids and minor Neoproterozoic granites.

Precambrian basement is mainly represented by the Paleoproterozoic Jinshuikou Group and the Mesoproterozoic Langyashan Formation. Jinshuikou Group can be subdivided into Baishahe and Xiaomiao formations based on distinctive rock associations and metamorphic grades. Baishahe Formation is characterized by paragneiss, amphibolites, marbles, and schists. Metamorphic pressure–temperature (P–T) conditions estimated for the paragneiss and amphibolite from the Baishahe Formation are P = 0.45−1.19 kbar and T = 638−896 °C [93]. Xiaomiao Formation consists of schists, quartzites, and marbles interlayered with minor metabasalts. Protoliths of these rocks were a suite of mudstones, quartz sandstones, and limestones deposited in a rift basin setting [94]. Metamorphic grades reach lower amphibolite facies. Recently, some researchers have suggested that Baishahe and Xiaomiao formations may be assigned to the Paleoproterozoic and Mesoproterozoic, respectively, based on the youngest detrital zircon ages of 2.2 Ga in the Baishahe Formation and 1.6 Ga in the Xiaomiao Formation [95,96]. Langyashan Formation is defined by a suite of carbonates, including dolomites, limestones, and minor siltstones, and phyllites [97]. Neoproterozoic strata are missing in the NKT.

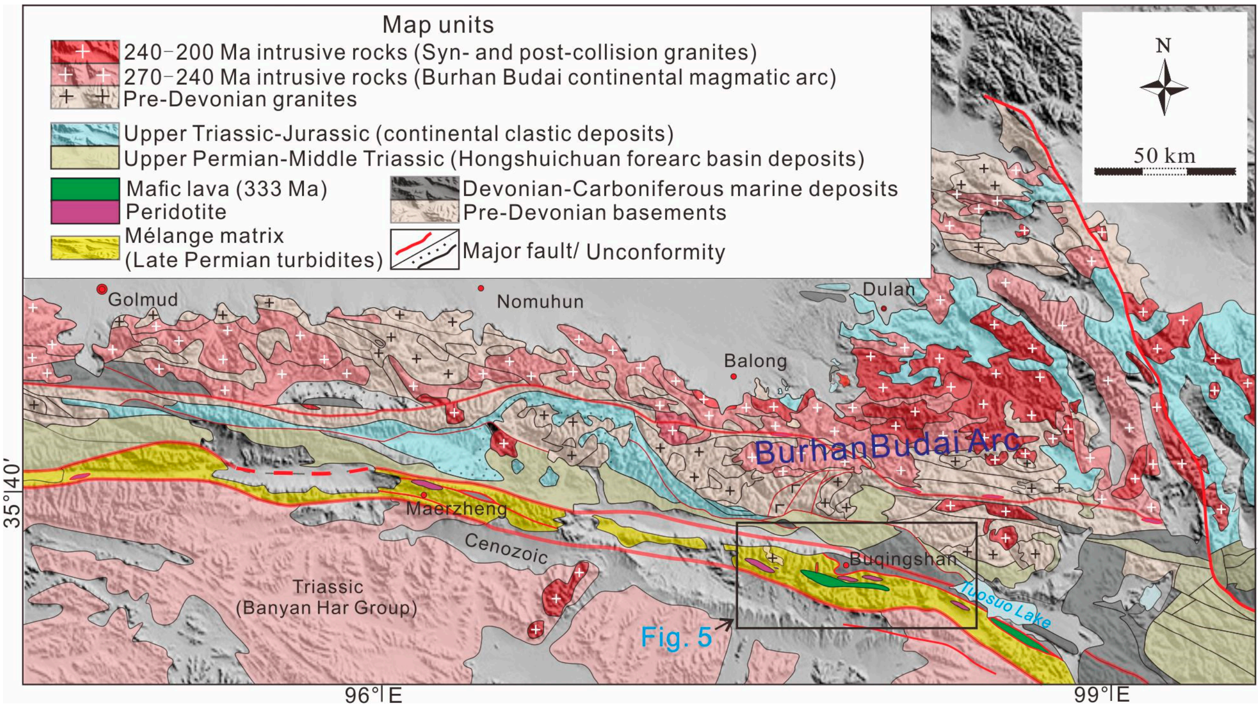

Figure 3. Geological map of eastern part of the East Kunlun Orogen.

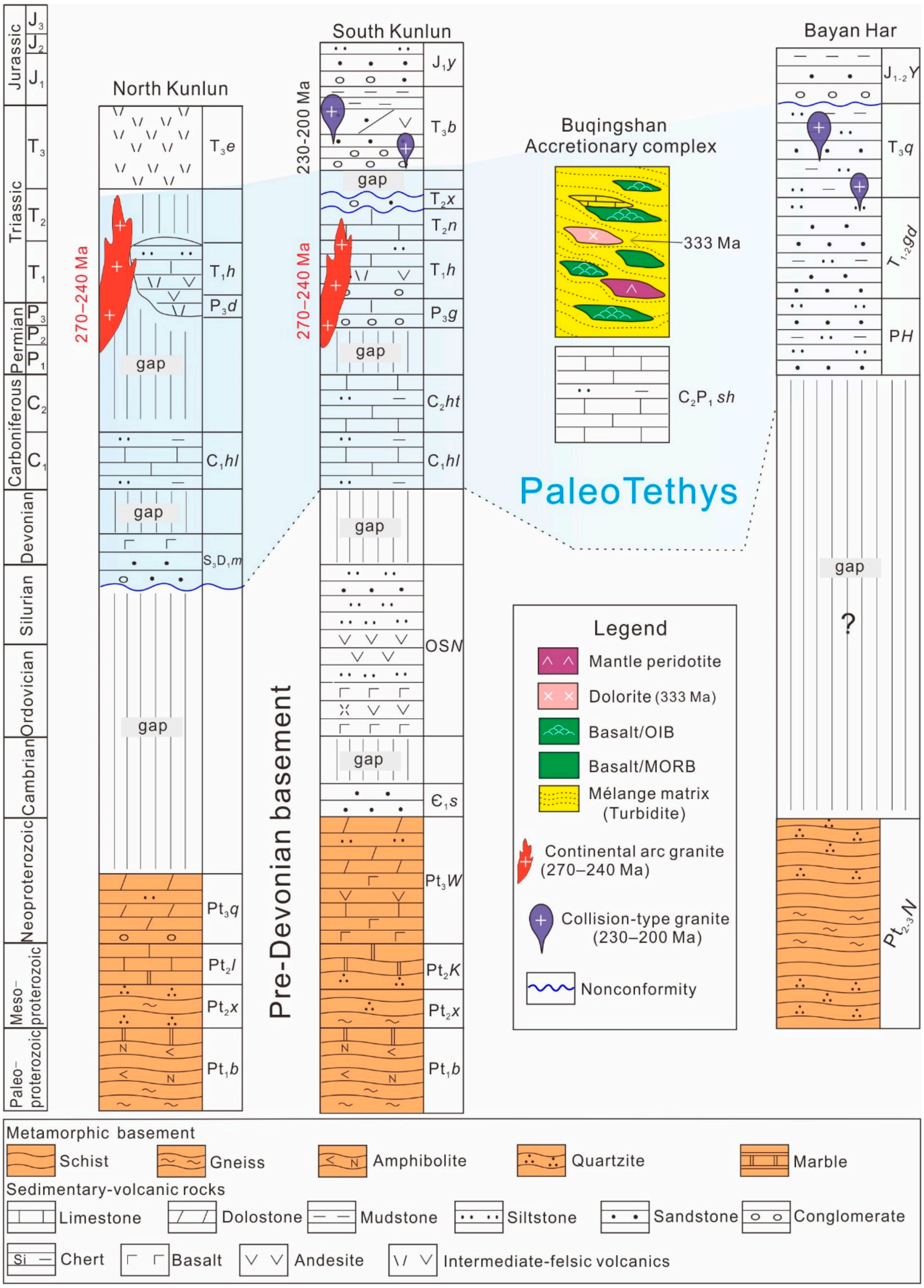

Figure 4. Stratigraphic columns for different tectonostratigraphic units in the East Kunlun orogen. No vertical scale. See text for more details. (Pt_1b—Paleoproterozoic Baishahe Formation; Pt_2x—Mesoproterozoic Xiaomiao Formation; Pt_2K—Mesoproterozoic Kuhai Group; Pt_2l—Mesoproterozoic Langyashan Formation; Pt_3W—Neoproterozoic Wanbaogou Group; Pt_3q—Neoproterozoic Qiujidong Formation; $Pt_{2\text{-}3}N$—Mesoproterozoic to Neoproterozoic Ningduo Group; $Є_1s$—Lower Cambrian Shasongwula Formation; OS*N*—Ordovician to Silurian Nachitai Group; Ss—Silurian Saishiteng

Formation; S_3D_1m—Upper Silurian to Lower Devonian Maoniushan Formation; C_1hl—Lower Carboniferous Halaguole Formation; C_2ht—Upper Carboniferous Haoteluowa Formation; C_2P_1sh—Upper Carboniferous to Lower Permian Shuweimenke Formation; $P_{1\text{-}2}m$—Lower to Middle Permian Maerzheng Formation; PH—Permian Hangyangling Group; P_3g—Upper Permian Gequ Formation; P_3d—Upper Permian Dazaohuo Formation; $T_{1\text{-}2}gd$—Lower to Middle Triassic Gande Formation; T_1h—Lower Triassic Hongshuichuan Formation; T_2n—Middle Triassic Naocangjiangou Formation; T_2x—Middle Triassic Xilikete Formation; T_3b—Upper Triassic Babaoshan Formation; T_3e—Upper Triassic Elashan Formation; T_3q—Upper Triassic Qingshuihe Formation; J_1y—Lower Jurassic Yangqu Formation; $J_{1\text{-}2}Y$—Lower to Middle Jurassic Yeerqiang Group).

Paleozoic metamorphic rocks are represented by the NaijTai Group composed of low-grade metamorphic volcanic-sedimentary rocks [98]. The Upper Silurian to Lower Devonian Maoniushan Formation (molasse strata) is restricted to the central fault of the EKO and includes conglomerates, sandstones, and siltstones, as well as minor bimodal basalt–rhyolite volcanics. These rocks are considered a molasse formed during a post-orogenic stage related to the closure of the Proto-Tethys Ocean [99].

In addition, HP-UHP metamorphic belts incorporating eclogites and granulites are exposed along the southern margin of the NKT. They have peak and retrograde metamorphic ages of 430–410 Ma. Coesite pseudomorphs in garnet, quartz exsolution rods in omphacite, and P-T calculations suggest that these eclogites experienced UHP metamorphic conditions at 29–30 kbar and 610–675 °C, possibly representing the final closure of the Proto-Tethys Ocean [19,26,100].

2.2. South Kunlun Terrane

The SKT consists of Precambrian basement, Neoproterozoic–Early Paleozoic metasedimentary–volcanic rocks (e.g., the NaijTai Group, Saishiteng Formation), widespread Late Paleozoic to Mesozoic sedimentary rocks, and minor Early Paleozoic and Late Permian–Triassic granites (Figures 3 and 4). The Precambrian basement includes the Baishahe and Xiaomiao formations and the Kuhai Group, the rock associations which are similar to those of the NKT. The Mesoproterozoic Kuhai Group is chiefly distributed in the eastern section of the SKT and characterized by schists, paragneisses, amphibolites, and marbles. This group is also part of the metamorphic basement.

The Wanbaogou and NaijTai groups are distributed mainly in the Northern SKT and composed of basaltic lavas, terrigenous and volcaniclastic rocks, and limestones. Some workers reported that the Wanbaogou Group formed around 762 Ma and that it developed in a continental rift or an incipient oceanic basin [101], representing the peak stage of Rodinia breakup and a precursor of the Proto-Tethys Ocean in the East Kunlun Ranges. Zircon U-Pb dating and geochemical study of the NaijTai Group shows that these rocks formed in an Early Paleozoic back-arc basin environment [98], which may have been related to the northward subduction of the Proto-Tethys Ocean.

Carboniferous successions consist of two distinct units named the Haleguole (Lower Carboniferous) and Haoteluowa (Upper Carboniferous) formations. The Haleguole Formation consists of fine-grained quartz sandstones, siltstones, and mudstones, grading upward into thin-bedded limestones. The Haoteluowa Formation comprises thin- to thick-bedded limestones and mudstones interlayered with sandstones. These successions were deposited in a littoral shallow marine environment on a passive continental margin, which formed in response to the opening of the Paleo-Tethys Ocean [102,103]. Widespread Upper Permian–Triassic strata overlie the pre-Permian strata with an angular unconformity and consist mainly of conglomerates, sandstones, siltstones, mudstones, and limestones.

2.3. Bayan Har Terrane

The BT is characterized by minor occurrences of the Mesoproterozoic Ningduo Group and Permian Huangyangling Formation and more widespread expanses of the Triassic Bayan Har Group. These are unconformably overlain by the Jurassic Yeerqiang Group (Figure 4). The Ningduo Group consists of paragneisses, schists and quartzites. The Huangyangling Formation is sparsely distributed in the northern part of the BT and consists of sandstones, slates, and minor interbedded volcanic rocks. The Bayan Har Group consists of the Lower to Middle Triassic Gande Formation and the Upper Triassic Qingshuihe Formation. The former is composed of medium-grained lithic arkoses and subarkoses interbedded with slates. These sedimentary rocks were deposited in bathyal to abyssal environments [104]. The Qingshuihe Formation incorporates sericitic slates, silty slates, and calcareous siltstones interlayered with sandstones and minor conglomerates at higher levels, representing sediments of a typical deep marine turbidite fan system.

2.4. Buqingshan Accretionary Complex

The Buqingshan AC is of a regional scale and separates the East Kunlun terrane to the north from the Bayan Har terrane to the south (Figure 2a). Geographically, it extends from Animaqen in the east, through Buqingshan, and into the Muztagh area in the west (Figure 2). It is characterized by a widespread mélange matrix with numerous tectonic blocks showing typical block-in-matrix structures [105,106] (Figures 5 and 6).

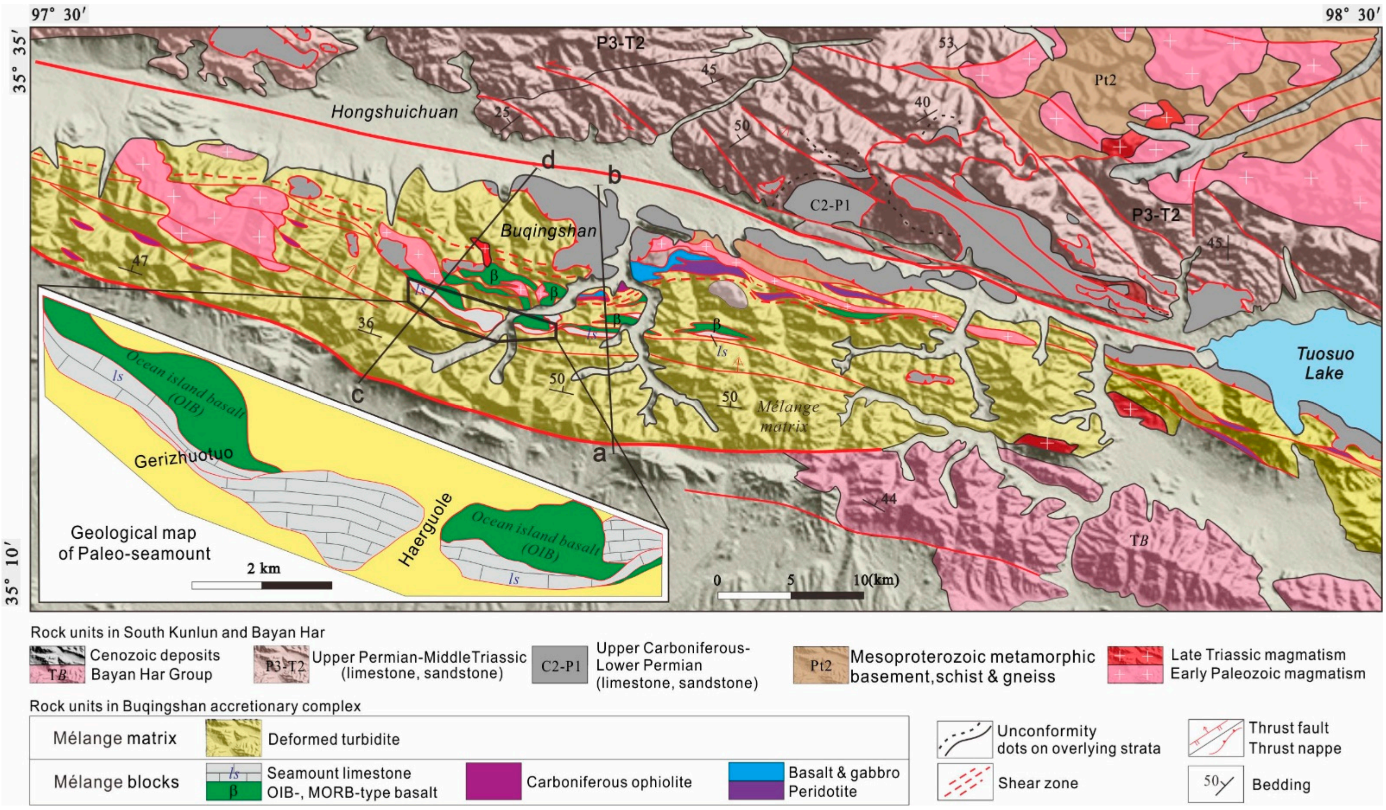

Figure 5. Geological map of the Buqingshan accretionary complex (see Figure 3 for location).

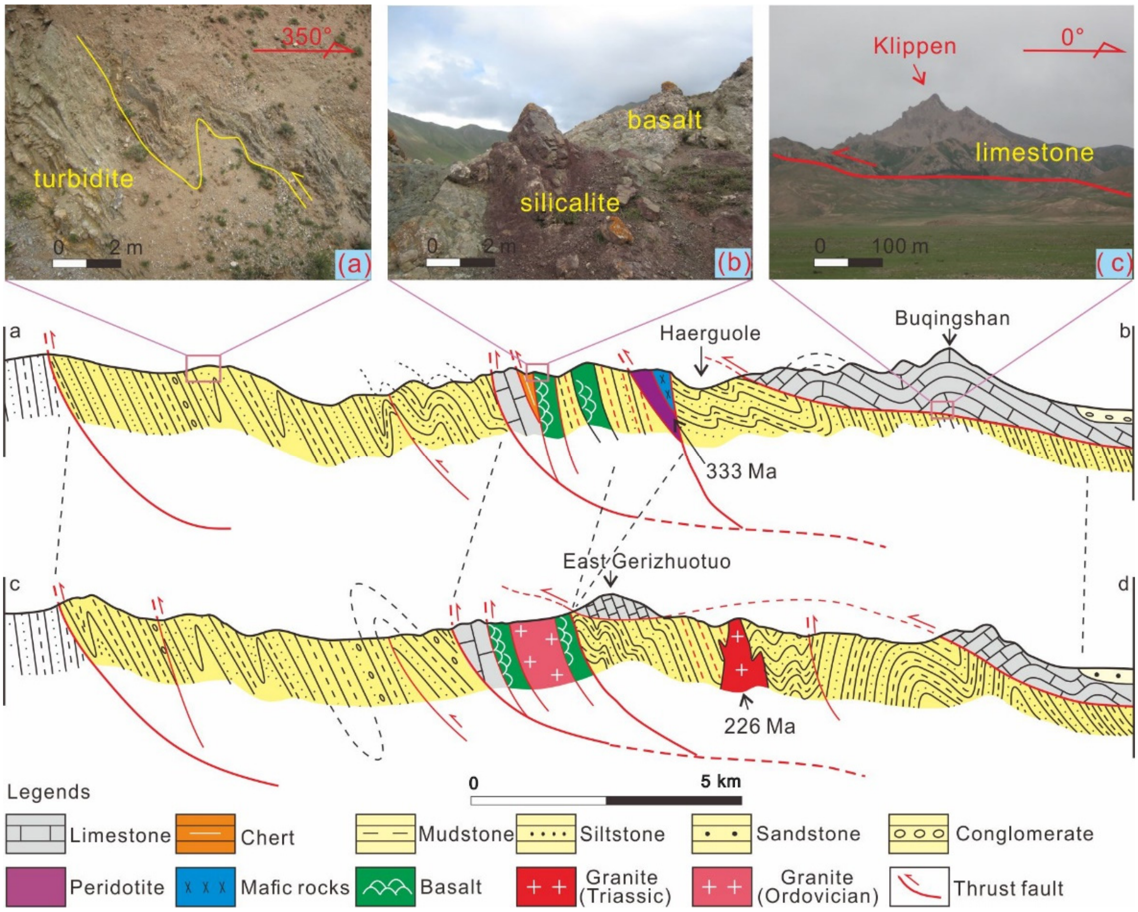

Figure 6. Geological cross sections for the Buqingshan accretionary complex showing block-in-matrix structure and structural style (age data are from Liu and Li [61,106]) (see Figure 5 for section location); (**a**) asymmetrical tight fold indicating south-vergent kinematics; (**b**) basalt and overlying silicalite; (**c**) Carboniferous limestone nappe thrust over deformed Permian turbidites.

The mélange matrix is typically composed of highly deformed turbiditic rocks, which are also referred to as the Lower to Middle Permian Maerzheng Formation in the literature [14] (Figures 6 and 7). In addition, Zhang et al. [107] suggested that the depositional age of the Maerzheng Formation ranges from Early Permian to Early Triassic based on the radiolarian fossil assemblages. This formation is characterized by a succession of medium-to coarse-grained sandstones, siltstones, and mudstones interlayered with minor conglomerates, which are deposited in a submarine fan setting. Their detrital zircon U-Pb spectra are dominated by ages of 396–573 Ma and 727–947 Ma with minor age peaks at 1117–1993 Ma and 2319–3063 Ma [14,108], suggesting a depositional source from pre-Devonian orogenic basement rocks of EKO. It is suggested that the turbidites were deposited in an oceanic trench environment and then incorporated into a subduction wedge. Recently, other workers suggested that some part of the Maerzheng Formation was originally deposited on a passive continental margin during Early–Middle Permian time and could have been tectonically incorporated into the Buqingshan AC [14,107]. However, it is a challenge to differentiate which part represents the trench in this mélange zone because of its similarity of rock associations in the field.

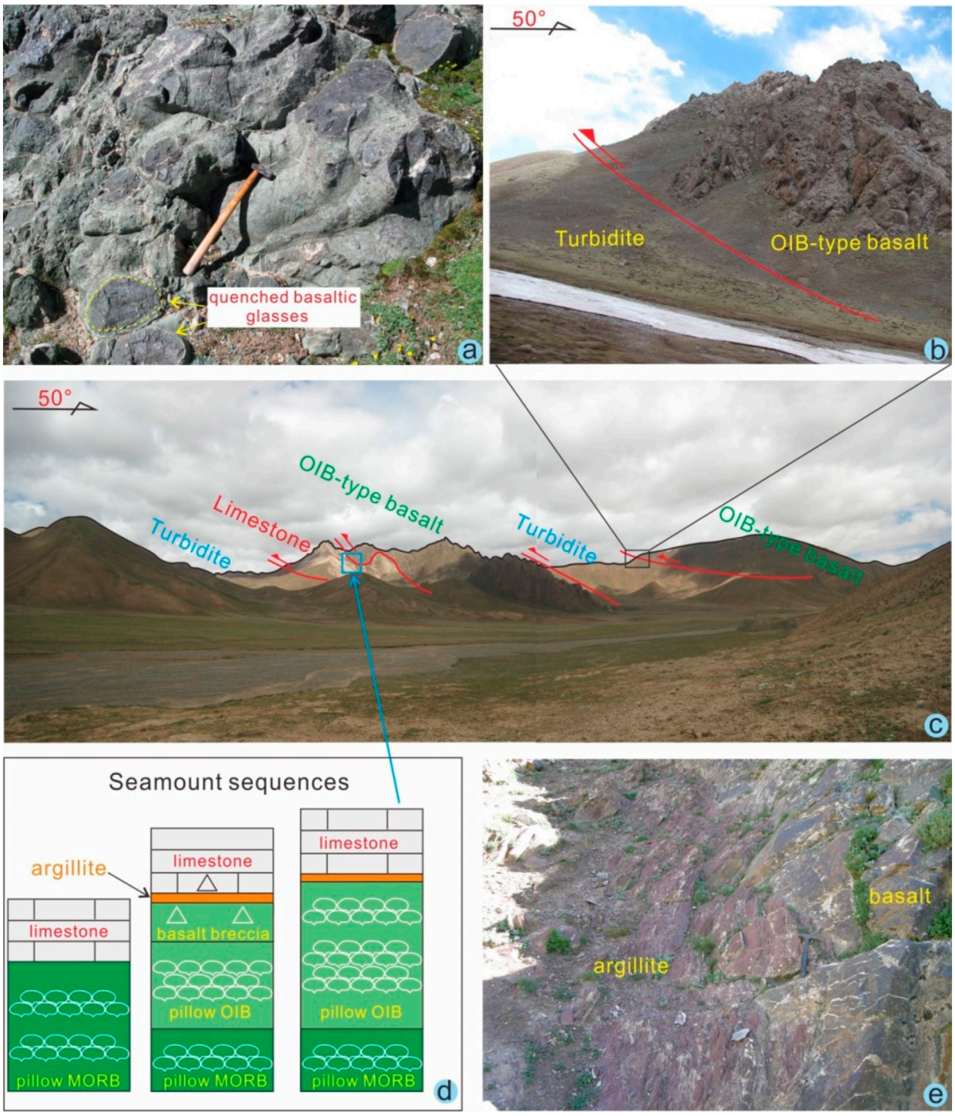

Figure 7. (**a**) Basalts exhibiting pillow structure and preserving quenched glass textures; (**b**) basalts thrust southward over strongly deformed turbidites; (**c**) paleo-seamounts preserving oceanic island basalts and a limestone cap incorporated into deformed turbidites; (**d**) seamount sequences with basaltic basement and limestone cap; (**e**) basalts within argillite-matrix mélange.

Mélange blocks mainly include fragments of Cambrian ophiolites, Carboniferous ophiolites and oceanic island basalts (OIBs), seamount limestones, with a minor contribution of the Mesoproterozoic metamorphic basement (Kuhai Group). The Cambrian ophiolites possibly indicate the existence of a much earlier Proto-Tethys Ocean that was tectonically incorporated into the Buqingshan AC during Triassic orogenesis [4,106]. Carboniferous ophiolites and oceanic island assemblages (basalts and limestones) record the spreading of the Paleo-Tethys Ocean in the EKO [2,106,109,110]. Kuhai Group metamorphic rocks could represent a continental slice that rifted from the SKT during the opening of the Paleo-Tethys Ocean. The detailed geochemistry and tectonic affinities of these blocks are discussed in Section 3 below.

3. Ocean Plate Stratigraphy in the Buqingshan AC

Ocean plate stratigraphy (OPS) is defined as the original composite stratigraphy of the ocean floor before it was incorporated into an accretionary complex (AC) at a convergent margin. It records the succession from the initiation of the oceanic plate at a mid-oceanic ridge to subduction at an oceanic trench [111–113]. A typical OPS section may consist of mantle peridotite, mid-ocean ridge basalt (MORB), ocean island basalt (OIB), seamount limestone, pelagic chert, hemipelagic siliceous shale, mudstone, and even rifted continental slices [114–116]. The identification of OPS in an AC allows one to reveal the evolution of paleo-oceans from their opening recorded in the OPS to their closure recorded in accretionary and collisional complexes [115].

Based on a field survey and previous data, OPS rock units in the Buqingshan AC are predominantly distributed in the Animaqen, Buqingshan, Maerzheng, and Muztagh areas from east to west (Figure 2a). They generally occur as isolated blocks sandwiched between deformed siltstones and sandstones (Figure 7a,c). In this study, we collated a total of 68 reliable published geochemical data points for the Buqingshan AC. These results show the geochemical diversity of the OPS sequences, such as depleted and refractory mantle peridotite, MORB- and OIB-type mafic rocks.

3.1. Mantle Peridotites

Ultramafic rocks from the Derni, East Haerguole, and Changliugou ophiolites are mostly altered to serpentinites or serpentinized lherzolites and harzburgites. Geochemically, they exhibit two distinct groups of mantle compositions. Peridotites in the East Haerguole area are mainly serpentinized harzburgites characterized by depletion in Al_2O_3, CaO, and TiO_2 and enrichment in MgO, indicating high degrees of mantle melting. In the chondrite-normalized rare earth element (REE) diagrams, these samples exhibit a V-shaped distribution pattern (Figure 8a), and the heavy REEs (HREEs) are closer to forearc mantle peridotites than to abyssal peridotites [117]. These characteristics indicate they represent relict mantle subjected to approximately 20–25% partial melting of the primitive mantle. In the primitive mantle-normalized trace element diagram (Figure 8b), these samples show enrichment in fluid-soluble elements (large ion lithophile elements (LILEs), Rb, Ba, U, and Th) and depletion in high field strength elements (HFSEs). Such features may suggest a refractory forearc mantle environment.

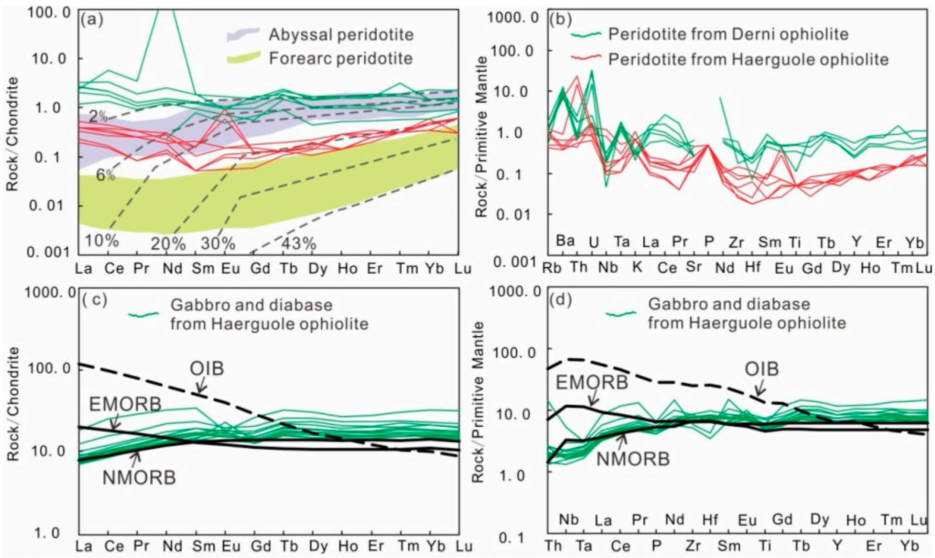

Figure 8. *Cont.*

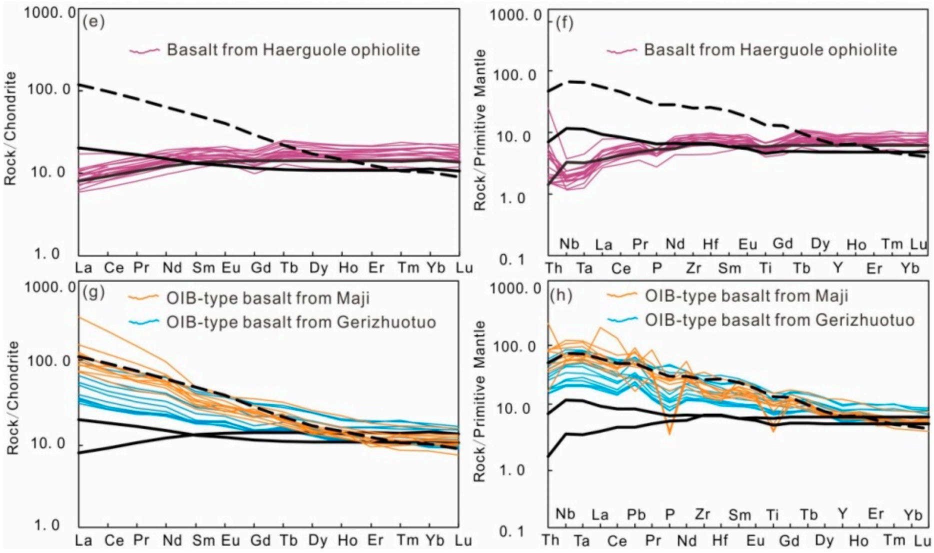

Figure 8. (**a**) Chondrite-normalized REE patterns for peridotites from Derni and Haerguole ophiolite; (**b**) primitive mantle-normalized trace element spider diagrams for peridotites from Derni and Haerguole ophiolite; (**c**) chondrite-normalized REE patterns for gabbros and diabases from Haerguole ophiolite; (**d**) primitive mantle-normalized trace element spider diagrams for gabbros and diabases from Haerguole ophiolite; (**e**) chondrite-normalized REE patterns for basalts from Haerguole ophiolite; (**f**) primitive mantle-normalized trace element spider diagrams for basalts from Haerguole ophiolite; (**g**) chondrite-normalized REE patterns for OIB-type basalts from Maji and Gerizhuotuo area; (**h**) primitive mantle-normalized trace element spider diagrams for OIB-type basalts from Maji and Gerizhuotuo area. Normalized values for chondrite and primitive mantle are from Boynton et al. [118] and Sun and McDonough [119]. Detailed geochemical data are presented in Supplementary Table S1. Representative data are from East Haerguole, Gerizhuotuo, Derni, and Maji areas [109,110,120–124].

In contrast, the mantle peridotites in the Derni and Changliugou areas are predominately serpentinized lherzolites characterized by relative enrichments in Al_2O_3, CaO, TiO_2, and depletions in MgO [124,125], pointing to lower degrees of mantle melting. The Cr# values (100∗Cr/(Cr + Al)) of spinel from the Derni ophiolite range from 30 to 57, which is identical to those of the abyssal mantle (<60). In the chondrite-normalized REE diagram, these samples show a weakly light REE (LREE)-rich distribution pattern (Figure 8a), and the HREEs are akin to abyssal mantle peridotites [117]. This further suggests that they represent a relict mantle that has undergone approximately 2–6% partial melting of the primitive mantle. These mantle peridotites are interpreted to have formed in a fast-spreading mid-ocean ridge environment during the Late Carboniferous time [124].

3.2. MORB-Type Oceanic Crust

Carboniferous–Permian MORB-type mafic rocks are mainly located in the Animaqen and Buqingshan regions. They are typically made up of pillow basalt, massive basalt, and fine-grained gabbro. They are characterized by low SiO_2, variable MgO, and high TiO_2 and are classified as tholeiitic series rocks. In particular, the TiO_2 contents are higher than those of island arc lavas (<1.0 wt.%) and lower than those of OIBs, whereas they are comparable to those of normal MORB (N-MORB) (=1.5 wt.%) [126]. In the chondrite-normalized REE patterns (Figure 8c,e), these samples exhibit overall depletion in LREEs relative to HREEs with REE patterns similar to that of the N-MORB reference line. In addition, they exhibit depletion in most LILEs and flat distribution of HFSEs without any Nb and Ta anomalies in the primitive mantle-normalized trace element spider diagrams, which also suggests N-MORB affinities (Figure 8d,f). On a tectonic setting discrimination diagram (Figure 9a), they predominantly plot within the mid-ocean ridge environment and show a depleted mantle source (Figure 9b). High $\varepsilon_{Nd}(t)$ values of +8.4 to +9.6 further support this conclusion [123].

Gabbros from the Buqingshan area yield an LA-ICP-MS zircon age of 333 ± 3 Ma [120], which is close to the Ar-Ar age of 345 ± 8 Ma [122,123], directly constraining formation ages to the Middle Carboniferous.

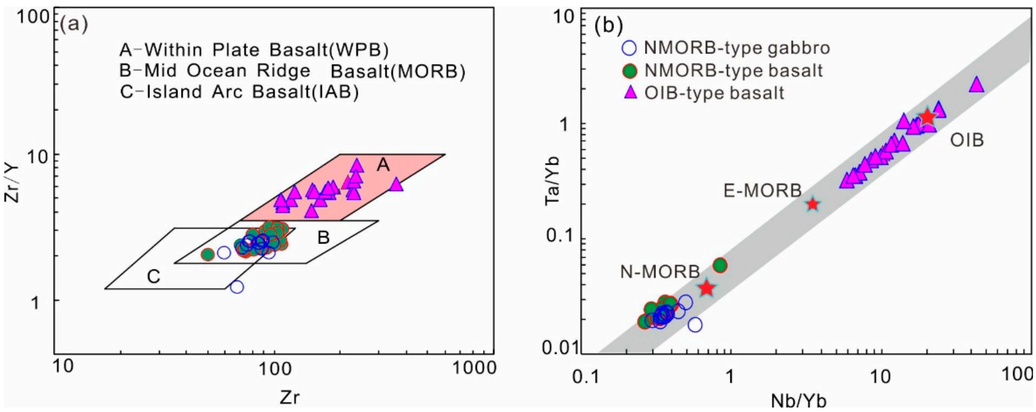

Figure 9. (**a**) Zr vs. Zr/Y and (**b**) Nb/Yb vs. Ta/Yb diagrams for mafic magmatic rocks.

3.3. OIB-Type Basalts and Seamounts

Seamount assemblages are mainly located in the Gerizhuotuo, Haerguole, and Majixueshan regions from west to east. They are typically made up of a basaltic basement overlain by cherts, limestones, and slope facies sedimentary rocks (Figure 7a,d). The basaltic basement consists of a pillow and massive basalts (Figure 7a). The carbonates comprise locally fossiliferous massive/micritic limestone (Figure 7c). The slope facies consist of basaltic and limestone breccias. They have similar characteristics to the well-described oceanic island/seamount associations worldwide [112].

Geochemically, the basalts are mainly characterized by low SiO_2, intermediate MgO, and high TiO_2 and are representative of the tholeiitic series. The TiO_2 contents are similar to those of OIBs (=2.0 wt.%) [126]. On chondrite-normalized REE patterns (Figure 8g) these samples exhibit enrichment in LREEs relative to HREEs with REE patterns similar to the OIB reference line. They also show enrichment in LILEs, Ti, Nb, and Ta in primitive mantle-normalized trace element spider diagrams, further suggesting OIB affinities (Figure 8h). On a discrimination diagram for tectonic settings (Figure 9a), all samples plot in the within-plate-basalt (WPB) field and show a similar affinity to OIB. Petrogenesis implies that they are the products of low-degree partial melting of lherzolite in the asthenospheric mantle [110,121,127]. Some researchers consider these basalts to have formed during the Carboniferous–Permian based on stratal relationships and whole-rock Rb-Sr age data (340 ± 11 Ma) [3,121].

Regionally, some researchers have reported other types of seamounts in the Animaqen and Bayan Har areas [109,128]. They consist of MORB basalt basement overlain by thick limestone (Figure 7d). These paleo-seamounts are considered to have formed in an area proximal to an uplifted mid-ocean ridge [14], which lay above the carbonate compensation depth (CCD). In the Southern Haerguole area, a paleo-seamount includes a suite of MORB, OIB, argillite, and massive/brecciated limestone from base to top (Figure 7d). This sequence formed in response at first to N-MORB-type magma extrusion near a mid-ocean ridge and then to superimposition of OIB-type magma followed by deposition of limestone [14,120,121].

4. Magmatic and Sedimentary Records of Subduction of the Buqingshan Ocean

The northward subduction of the Buqingshan Ocean led to the development of an extensive W–E-trending continental magmatic arc (Burhan Budai arc), forearc basin (Hongshuichuan Basin), accretionary complex (Buqingshan AC) (Figures 2a and 5), and an immature back-arc basin during Late Permian to Middle Triassic times. We collected some geochemical analyses from the EKO in order to characterize the nature of continental arc magmatism and sedimentation within the forearc basin.

4.1. Continental Arc Magmatism

The 275–240 Ma Burhan Budai arc is mostly located in the NKT, with subordinate exposures in the SKT (Figure 2). Rocks associated with this arc crop out in the E–W direction with a linear distribution pattern (Figure 3), similar to the Gangdese magmatic arc in Tibet [129] and the Andean magmatic arc of South America [130,131]. They intruded into Precambrian metamorphic rocks and pre-Devonian granitoids (Figure 10a). The magmatism shows a large compositional range comprising granodiorites, granites, monzogranites, dark-colored microgranular enclaves (Figure 10b), and intermediate–felsic volcanics. Geochemically, these rocks are characterized by relatively high SiO_2, Na_2O, low MgO, and TiO_2 and are classified as high-K calc-alkaline metaluminous I-type granitoids. On the trace element spidergram (Figure 11), they are characterized by enrichment in LILEs (Cs, Rb, Ba, etc.), and depletion in HFSEs (e.g., Nb, Ta, Ti, etc.), similar to subduction-related arc rocks. On several discrimination diagrams for tectonic settings (Figure 12), these rocks mostly plot within the volcanic arc granite (VAG) field.

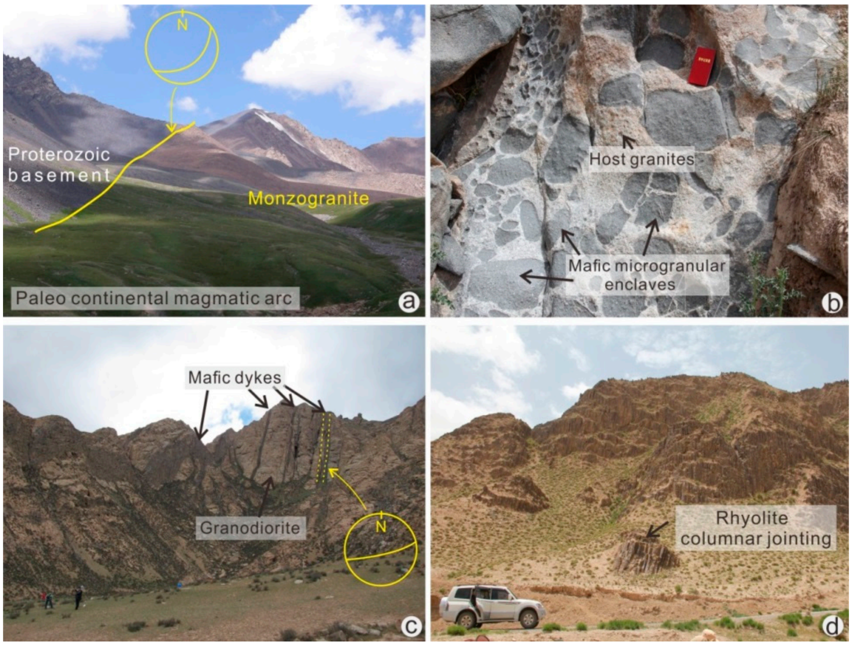

Figure 10. (**a**) Monzogranites intruding the Proterozoic basements (biotite quartz schist), (**b**) Early Triassic host granites and dark microgranular enclaves showing evidence for magma mixing, (**c**) Late Permian dyke swarm intruded into nearly coeval magmatic arc (granodiorite) rocks, and (**d**) Late Triassic post-collisional rhyolite exhibiting columnar jointing.

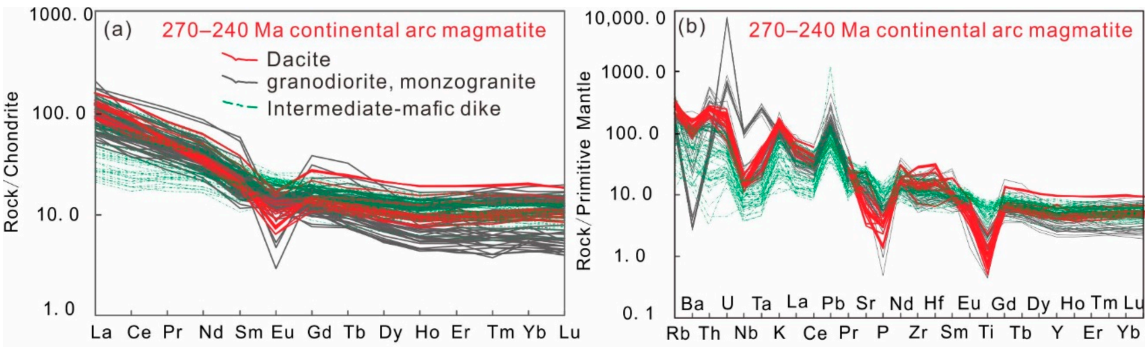

Figure 11. *Cont.*

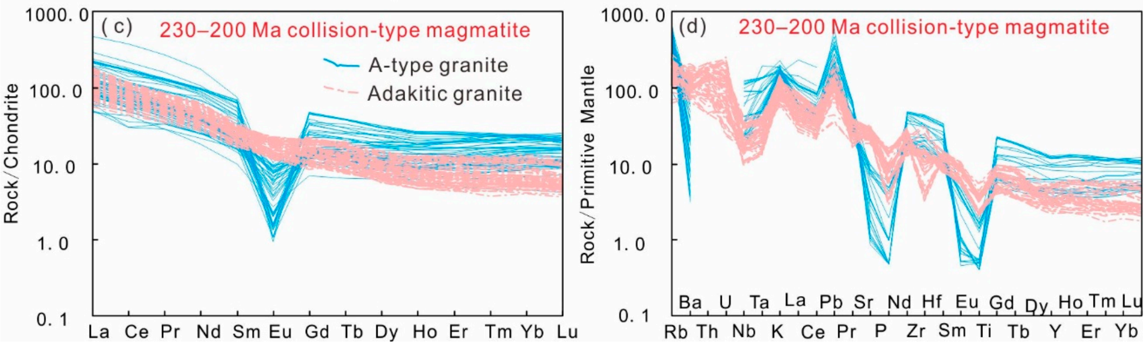

Figure 11. (**a**) Chondrite-normalized REE patterns for arc magmatic rocks; (**b**) primitive mantle-normalized trace element spider diagrams for arc magmatic rocks; (**c**) chondrite-normalized REE patterns for collisional-type rocks; (**d**) primitive mantle-normalized trace element spider diagrams for collisional-type rocks. Normalized values for chondrite and primitive mantle are from Boynton et al. [118] and Sun and McDonough [119], respectively. Geochemical data are presented in Supplementary Table S2.

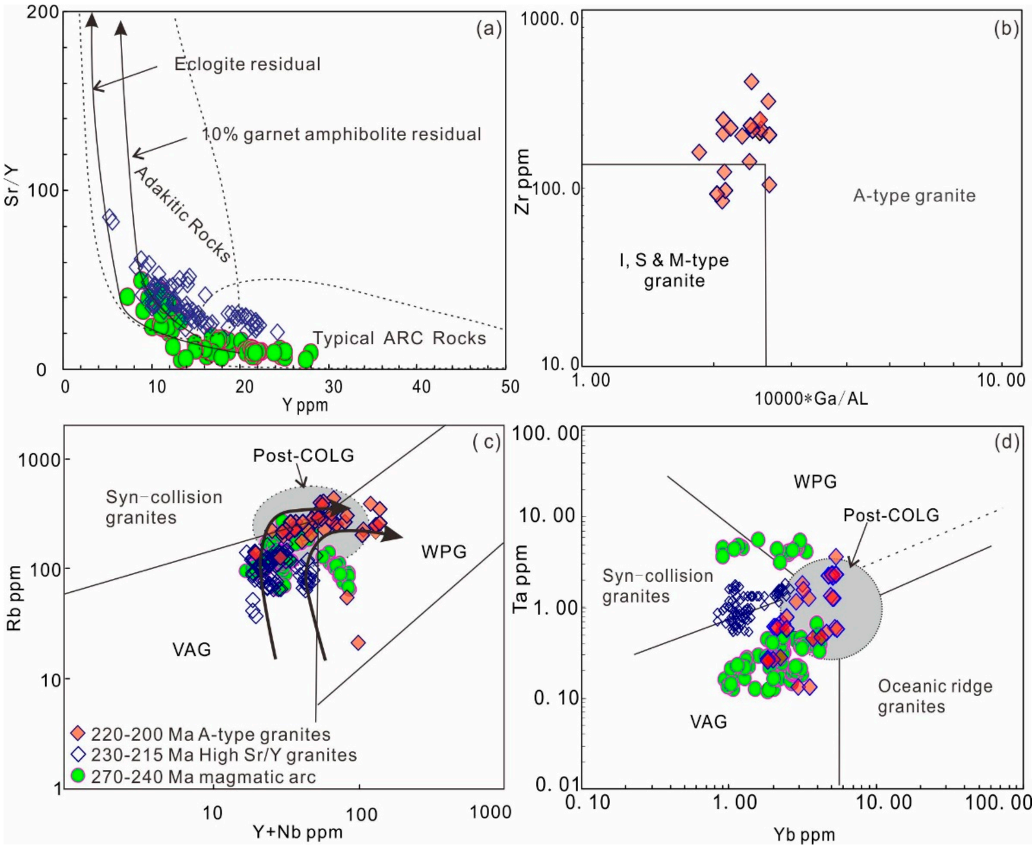

Figure 12. Tectonic discrimination diagrams for the Late Paleozoic–Triassic granitoids. (**a**) Y vs. Sr/Y (Defant et al. [132,133]), (**b**) 1000∗Ga/Al vs. Zr (Whalen et al. [134]), (**c**) Y + Nb vs. Rb (Pearce et al. [135]), and (**d**) Yb vs. Ta diagrams (Pearce et al. [135]). VAG—volcanic arc granite, WPG—within plate granite, COLG—collisional granite.

Voluminous contemporaneous intermediate and mafic dike swarms also developed within the aforementioned granitoids (Figure 10c). Compositionally, the dikes are mainly porphyritic diabases, lamprophyres, and diorite porphyries. Detailed mineralogical and geochemical studies showed that mafic dikes were derived from an enriched mantle (EM2-type mantle), and intermediate dikes were the result of mixing between mafic and felsic magmas above the subduction zone [136]. Regarding the mechanism of their formation, it is suggested that mafic magmas may have first been generated by the partial melting of the enriched subcontinental lithospheric mantle (SCLM) due to the addition of subduction zone-derived fluids above the northward-subducting plate [136]. These mafic magmas underplated the overlying lower crust and led to partial melting to form felsic magmas. The two distinct types of magma mingled extensively to produce the "mixed magmas" with consistent negative $\varepsilon_{Nd}(t)$ and $\varepsilon_{Hf}(t)$ isotopic values (Figures 10b and 13) [46,49,64,137,138]. The mafic microgranular enclaves (MMEs) and their host magma were then emplaced at a depth of ~12 km, where they crystallized at temperatures of ca. ~700–770 °C [28].

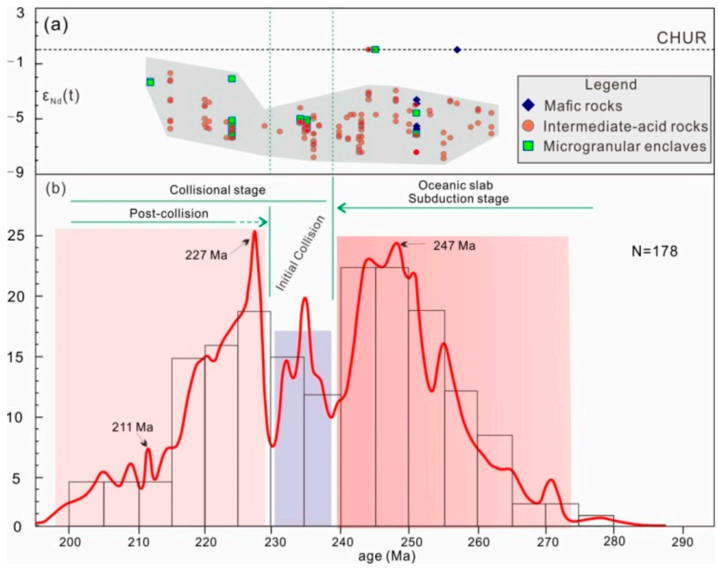

Figure 13. (**a**) Plot of formation age (Ma) and ε_{Nd} (*t*), and (**b**) zircon U-Pb age data histograms and probability density curves for the Late Paleozoic–Early Mesozoic magmatic rocks. The values of ε_{Nd} (*t*) from Yu et al. [22]. Age histograms are from Li [139].

Recently, Zhao et al. [80] reported 266 Ma tholeiitic gabbros from the central part of the Burhan Budai arc (i.e., the Kengdenongshe area). Based on their REE signature, the gabbros are thought to have formed in a back-arc basin. However, no true oceanic relicts of the Late Permian–Early Triassic back-arc basin are known from the EKO. Thus, we suggest that these dike swarms probably represent a localized extensional setting within a continental magmatic arc or an immature back-arc basin geodynamically related to the rollback of the subducting slab.

4.2. Forearc Basin

4.2.1. Sedimentary Successions

The Hongshuichuan forearc basin includes the Upper Permian Dazaohuo/Gequ, Lower Triassic Hongshuichuan, and Middle Triassic Naocangjiangou formations from base to top (Figures 3 and 14).

Geological field mapping shows that the Dazaohuo Formation occurs in the Western NKT and consists of intermediate–felsic volcanic rocks with continental arc affinities [91]. The Gequ Formation unconformably overlies the Middle Lower Permian Maerzheng Formation and is characterized by conglomerates, sandstones, and siltstones in the lower part and limestones in the upper part [39]. It was probably deposited in an initial filling stage of the forearc basin or during the transition from a passive to an active continental margin.

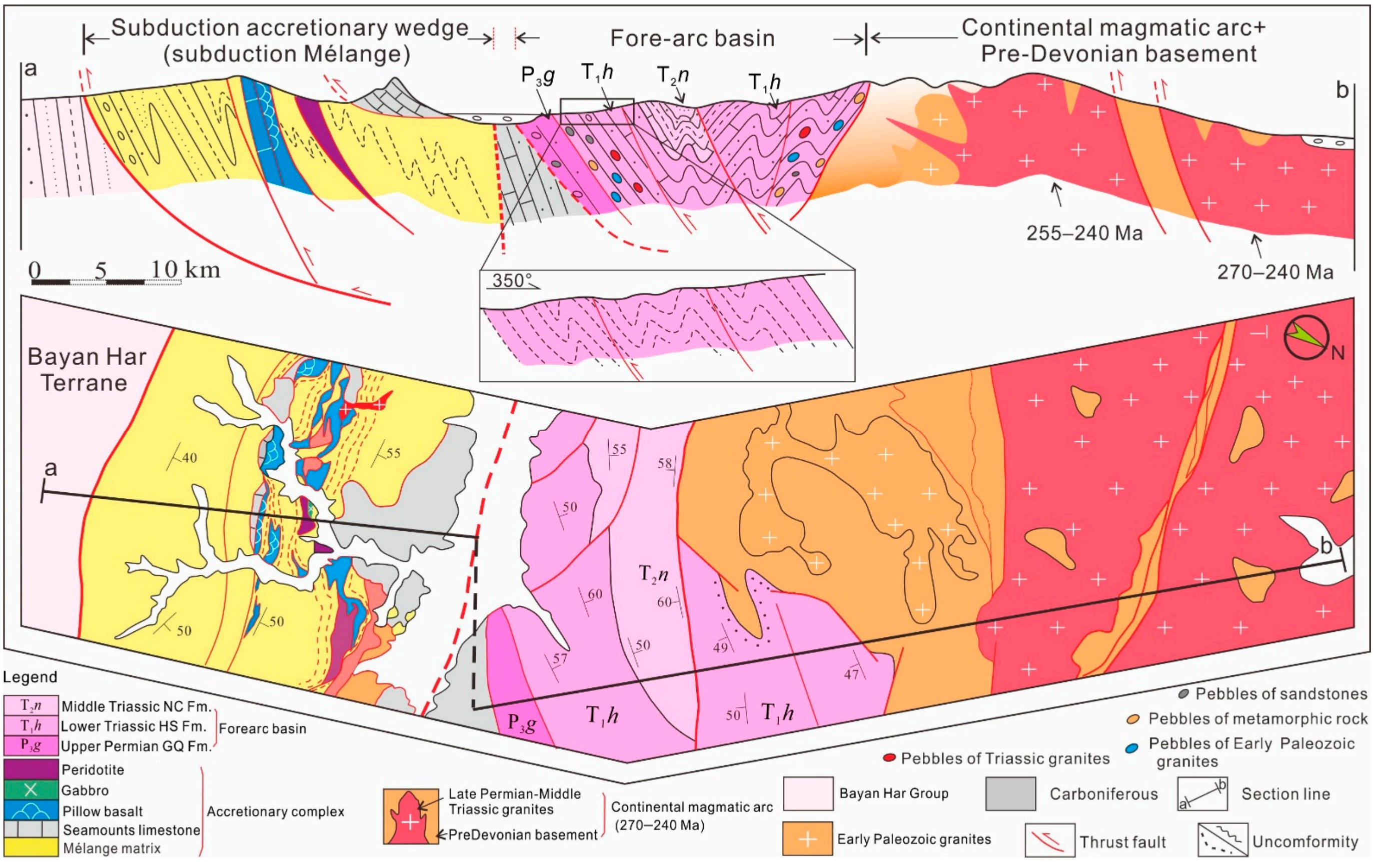

Figure 14. Map of geological transect and accompanying cross-section through the East Kunlun Orogen showing the Buqingshan accretionary wedge, Hongshuichuan forearc basin, and Burhan Budai continental arc from south to north.

The Hongshuichuan Formation can be subdivided into four units from base to top based on distinct rock associations and sedimentary structures. The first unit is characterized by red and gray–green polymictic conglomerates, sandstones, and minor tuffaceous siltstones generally with cross-bedded structures (Figure 15a,b), indicating a fan-delta environment [139]. The conglomerates are matrix- to clast-supported and composed of predominantly granite, metamorphic, and sandstone clasts with minor rhyolite, limestone, and silicic rock clasts (Figures 15b and 16). They have an average total quartz–feldspar–lithic fragment ratio of Q59:F32:L10 (Figure 16) [62]. The second unit is composed of gray sandstones intercalated with minor gray–black thin limestones and felsic volcanics possibly deposited in an agitated shallow marine environment (Figure 15e). The average total quartz–feldspar–lithic fragment ratio of the sandstones is Q40:F31:L28 [62], showing a gradual increase in feldspar and lithic fragments relative to the first unit. Beds in the third unit exhibit characteristic Bouma sequences and include a succession of thin black mudstones, siltstones, and tuffaceous sandstones interbedded with minor fine-grained conglomerates (Figure 15c). Together with typical sedimentary structures (e.g., Bouma sequences, graded bedding, convolute bedding, and load casts) (Figure 15d), these features suggest that the third unit was deposited by turbidity currents in a submarine fan environment. The average total quartz–feldspar–lithic fragment ratio is Q39:F36:L25 (Figure 16) [62]. These sandstones are moderately sorted with angular–subangular grains, which indicates immaturity characteristic of proximal and rapid deposition [139,140]. The fourth unit consists of gray thin fine-grained siliciclastic rocks locally interbedded with thin limestones and minor conglomerates, interpreted to have been deposited in a shallow marine environment.

The Naocangjiangou Formation conformably overlies the Hongshuichuan Formation and is characterized by gray mudstone, calcareous siltstone, and limestone associations

(Figure 15f,g). In detail, the lower part of the Naocangjiangou Formation is composed of mudstone and calcareous siltstone interbedded with thin limestone and continental arc volcanics with zircon ages of 244 Ma [141]. In contrast, the upper part is dominated by limestone with minor siltstone generally developing horizontal bedding structures. These strata were mainly deposited in shallow marine environments (Figure 15g), representing the final filling of the forearc basin [139]. The average total quartz–feldspar–lithic fragment ratios from the lower and upper parts are Q53: F21: L26 and Q48: F25: L27, respectively [62], showing higher feldspar and lithic fragment contents and low mineral and compositional maturity, which points toward a proximal source.

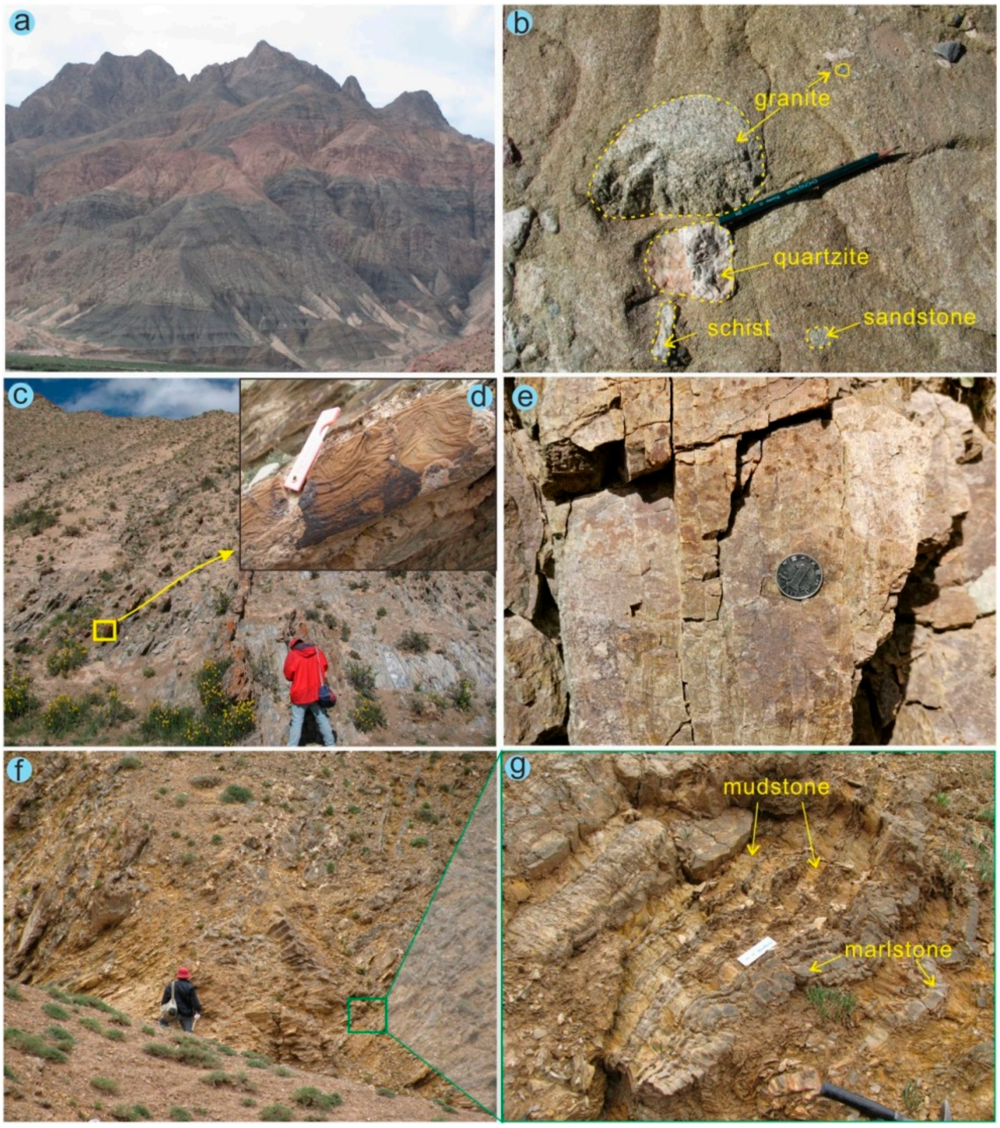

Figure 15. Field photographs showing the sedimentary characteristics of Late Permian–Middle Triassic Hongshuichuan forearc basin: (**a**) the fan-delta deposition of the lower part of the Hongshuichuan Formation; (**b**) pebbly feldspathic sandstone from the Hongshuichuan Formation showing pebbles of granite, quartzite, schist in a matrix of medium-grained sandstone; (**c**) rhythmically bedded sandstone, siltstone, and minor mudstone turbidite units with a variable thickness of 10–60 cm; (**d**) soft-sediment deformation showing convolute bedding in turbidite; (**e**) light colored rhyolite occurs as intercalations in Hongshuichuan Formation (taken in Zhanhongshan area). Naocangjiangou Formation: (**f**) rhythmic alternations of mudstone and marlstone with a variable thickness of 5–40 cm; (**g**) thin limestones interlayered with minor mudstones.

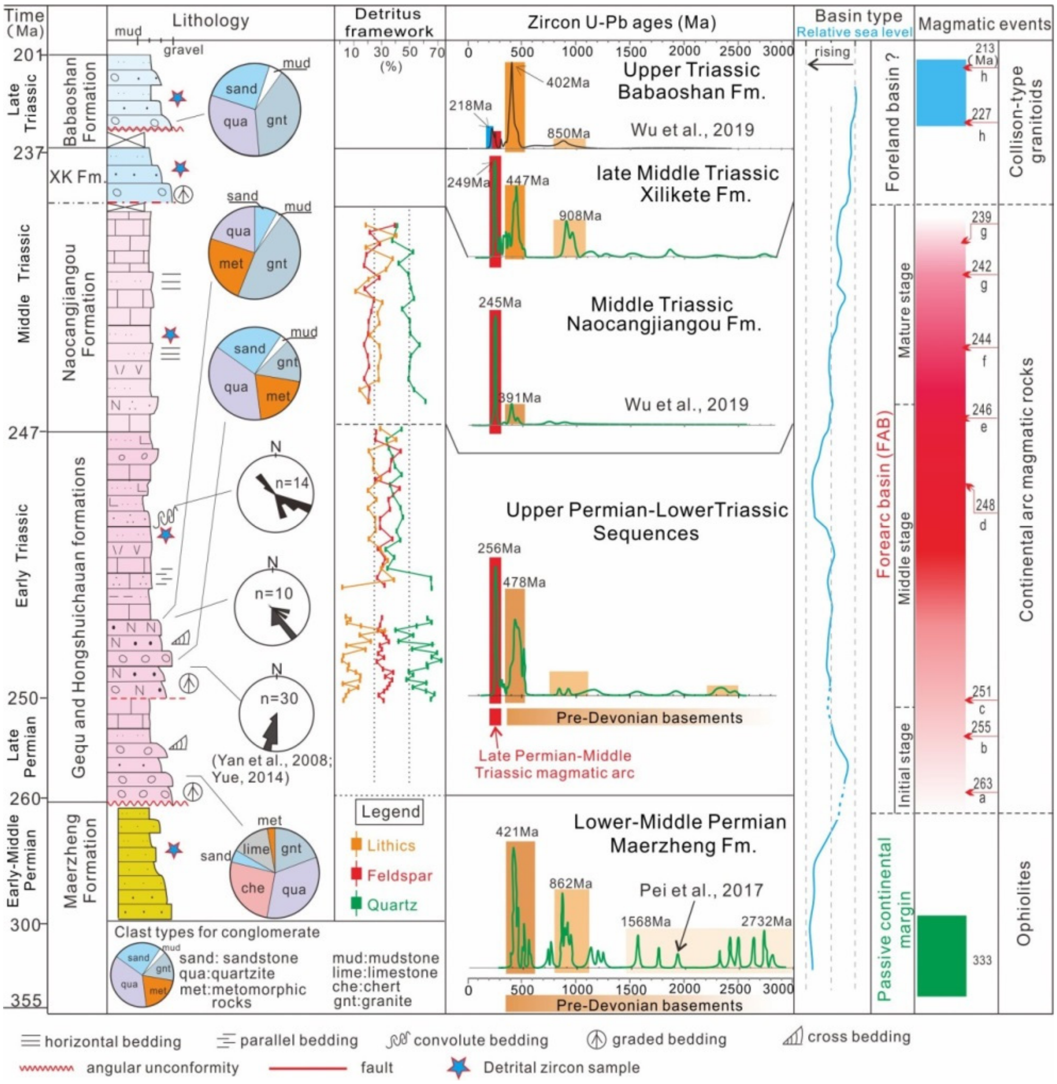

Figure 16. Summary of Late Paleozoic–Early Triassic sedimentary successions, sandstone detritus framework, and detritus zircon ages spectrum. XK Fm.-Xilikete Formation (magmatic events from Li et al. [49,50]; Age data of Babaoshan and Naocangjiangou formations from Wu et al. [20]; Age data of Maerzheng Formation from Pei et al. [14]).

4.2.2. Detrital Zircon Age Constraints on Sediment Provenance

Detrital zircon age spectra are commonly used to constrain both sediment provenance and the tectonic setting where the basin developed. In general, a basin developed in a convergent setting has a high proportion of detrital zircons with ages close to the age of the sediment. A basin developed in an extensional setting is dominated by detrital zircon ages that are typically much older than the depositional age of a unit with some proportion of grains having ages within 150 Ma of the depositional age [142].

Numerous detrital zircon U-Pb ages chiefly from the Permian to Triassic strata were compiled in order to reveal any systematic variations in provenance and shifts in basin type following the classification of Cawood et al. [142] (Figure 16). In order to characterize how sediment provenance and basin types change before/during a period of oceanic subduction, we also present a detrital zircon spectrum from a passive continental margin for comparison (i.e., Lower to Middle Permian Maerzheng Formation).

Sandstones from the Maerzheng Formation are dominated by Early Paleozoic age populations (peak age, ca. 421 Ma) and some Precambrian age populations (peak ages, ca. 862 Ma 1568 Ma, and 2732 Ma). This age distribution suggests a source exclusively from the pre-Devonian basement rocks in the EKO, including Early Paleozoic igneous rocks and Precambrian metamorphic basement rocks. This age spectrum shows similarity to that of detrital zircons from the extensional basins [142]. Pei et al. [143] argued that they were deposited on the passive continental margin basin related to the spreading of the northern branch of the Paleo-Tethys Ocean.

In contrast, the Upper Permian to Middle Triassic sandstones yield substantially lesser proportions of pre-Devonian ages and show a sharp increase in the Late Permian–Middle Triassic ages (ca. 277–244 Ma) representative of the well-known Burhan Budai continental magmatic arc in EKO [12,139,140]. In particular, the Middle Triassic Naocangjiangou Formation is characterized by more abundant Late Permian–Middle Triassic ages and minor pre-Devonian ages relative to those of the underlying strata (Hongshuichaun and Gequ formations), possibly implying more intense continental arc magmatism and progressive unroofing of the continental arc during the Middle Triassic, which in turn provided large volumes of detritus to the basin. Paleocurrent directions are predominantly SE and subordinately NW directed [144,145] indicating the derivation of detritus from the continental magmatic arc to the north and the Buqingshan AC to the south (Figure 14).

Accordingly, with detritus mainly sourced from the coeval magmatic arc, together with the paleocurrent directions and a location between the Buqingshan AC and Burhan Budai arc (Figures 14 and 17), this suggests a forearc basin setting for Upper Permian–Middle Triassic strata.

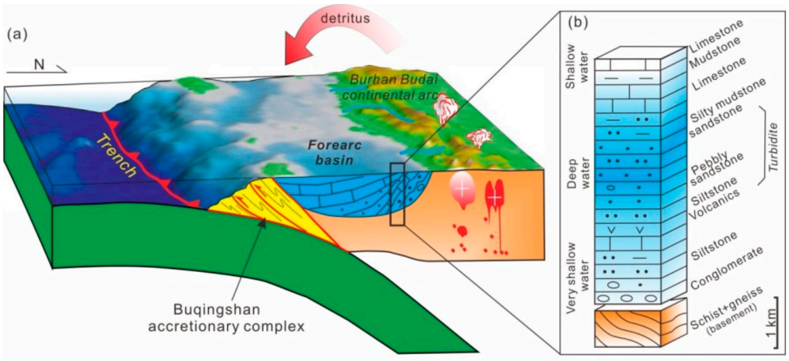

Figure 17. (**a**) Block diagram showing the Hongshuichuan forearc basin and oceanic subduction zone (modified from Frisch et al. [146]); (**b**) Integrated stratigraphic column of the forearc basin deposits during Late Permian to Middle Triassic time.

5. Magmatic and Sedimentary Records of Collisional Orogenesis

During the latest Middle Triassic, the closure of the Paleo-Tethys Ocean led to collisional orogenesis in the EKO and was accompanied by large volumes of collisional-type magmatic rocks and metallic mineral deposits.

5.1. Collision-Related Magmatism

The ca.240–200 Ma collisional-type magmatic rocks are haphazardly scattered across the whole EKO and BT unlike the linear distribution of continental arc granites (Burhan Budai arc) (Figure 3). They mainly intrude Lower to Middle Triassic sedimentary strata and include granites, diorites, gabbros, and minor syenogranites in lithology. In addition, large volumes of Late Triassic rhyolites occur in the Xiangride-Boluositai area (Figure 10d).

Geochemistry indicates the presence of adakitic, A-type, and normal granitic rocks [47,48,147,148]. Adakitic granites are characterized by enrichments in LREE, particularly high Sr, low Y, and Yb contents, high Sr/Y (>40) and La/Yb ratios, and depletions in Nb, Ta, and Ti [133,149] (Figure 11c,d). No Eu anomalies are notable in the chondrite-normalized REE patterns. On the Sr/Y vs. Y diagram, they predominantly plot in the field of adakitic rocks (Figure 12a), which are considered to be produced by partial melting of the thickened lower crust in syn-collisional and post-collisional tectonic environments [150]

(Figure 12c,d). Some researchers have reported ca. 227 Ma undeformed adakitic rocks in the Kekealong-Gerizhuotuo area [149] (Chen et al., 2013a), which constrains the time of regional crustal thickening. A-type granites have high SiO_2 and alkalis contents and high 10,000∗Ga/Al ratios, together with depletions in Sr, P, Eu, and Ti on the trace element spidergram, suggesting an affinity with A-type granites (Figure 12b). They predominantly plot in the post-collisional fields on the Y + Nb vs. Rb and Yb vs. Ta diagrams (Figure 12c,d).

This stage of magmatism can be further divided into two subgroups, namely, initial collisional/syn-collisional magmatism at ca. 240–230 Ma and post-collisional magmatism after ca. 230 Ma, based on distinct geochemical differences and a compilation of zircon ages (Figure 13). The histogram reveals that syn-collisional magmatism was less extensive than post-collisional magmatism. This is interpreted to indicate that the compressional conditions in the syn-collisional orogeny stage were not conducive to the production of voluminous magmas [47,48,151]. In contrast, post-collisional magmatism flared up at ca. 230 Ma and generated large volumes of adakitic and A-type granites as well as some metallic mineral deposits [152,153]. This is interpreted to be geodynamically related to mantle upwelling due to the detachment of thickened lithosphere [47,48].

5.2. Orogenic Sedimentation

5.2.1. EKO Sedimentary Records

Available geologic data show the sedimentary environment in the East Kunlun Range experienced a transition from marine facies in the Middle Triassic Naocangjiangou Formation to continental facies in the upper Middle Triassic Xilikete and Upper Triassic Babaoshan formations. The Xilikete Formation unconformably overlies the marine Naocangjiangou Formation [39,139], starting with a suite of red–gray conglomerates and sublitharenites with minor siltstones, and continuing into a succession of quartz sandstones, siltstones locally interbedded with pebbly sandstones and rhyolites at higher levels, which are interpreted to have formed in an alluvial fan environment.

The Babaoshan Formation, unconformably overlying the Middle Triassic Naocangjiangou Formation and the Precambrian basement comprises three suites of distinct depositional associations from base to top (Figure 16). The lower part is 284 to 533 m thick and characterized by thick pebbly subarkoses interbedded with minor conglomerates and siltstones. The middle part is up to 586 m thick and consists of thin, muddy siltstones and quartzose siltstones interlayered with minor fine-grained subarkoses. The upper part is >155 m thick and defined by fining-upward cyclical sequences of conglomerates, pebbly sandstones, fine-grained sandstones, and siltstones. Conglomerates are well-sorted with well-rounded clasts and basal erosion surfaces are locally developed. Sandstones are characterized by graded and trough cross-bedding. Siltstones show planar cross-bedding and horizontal bedding. These sedimentary features suggest deposition in a braided river system.

The detrital zircon U-Pb age spectra from the sandstones mentioned above suggest Late Triassic, Late Permian–Middle Triassic, and pre-Devonian EKO provenance (Figure 16). Notably, detritus with ages of ca. 400–1000 Ma reappears in the Xilikete and Babaoshan formations suggesting a recycled pre-Devonian basement. This may relate to the extensive uplift and erosion of the pre-Devonian strata during Late Triassic collisional orogenesis. Moreover, the abrupt appearance of ca. 218 Ma peak ages in Upper Triassic strata suggests that Late Triassic collision-related magmatic rocks began to contribute some sedimentary debris. Accordingly, it is suggested that the Babaoshan Formation was deposited in a piggyback or foreland basin in response to the collision of the East Kunlun terrane to the north with the Qiangtang/Bayan Har terranes to the south [139].

5.2.2. Bayan Har Terrane Sedimentary Records

The Bayan Har Group, mainly located in the BT, consists of the Lower to Middle Triassic Gande Formation and Upper Triassic Qingshuihe Formation. They are characterized by thick medium-grained lithic arkoses and subarkoses interbedded with slates and were deposited in bathyal, abyssal, and neritic environments. According to paleocurrent indicators and detrital zircon age data [12,104], paleocurrents in the northern part of the Bayan Har basin flowed in a predominantly SE direction. The detrital zircon age spectrum features dominant Precambrian and Paleozoic age peaks, showing detritus was mainly sourced from East Kunlun and West Qinling orogens to the north. Zhang [104] argued that the lower part of the Bayan Har Group formed in a residual ocean basin. The middle to the upper part of this group was deposited in a peripheral foreland basin that developed in response to the collision of the Qiangtang terrane with the East Kunlun terrane.

6. Tectonic Evolution of the Late Paleozoic–Mesozoic Buqingshan Ocean

Data presented and summarized in this investigation indicate that the Buqingshan Ocean spread in the Carboniferous followed by subduction of associated oceanic lithosphere culminating in the collision of Qiangtang/Bayan Har with the East Kunlun terranes and associated orogenesis (Figure 18).

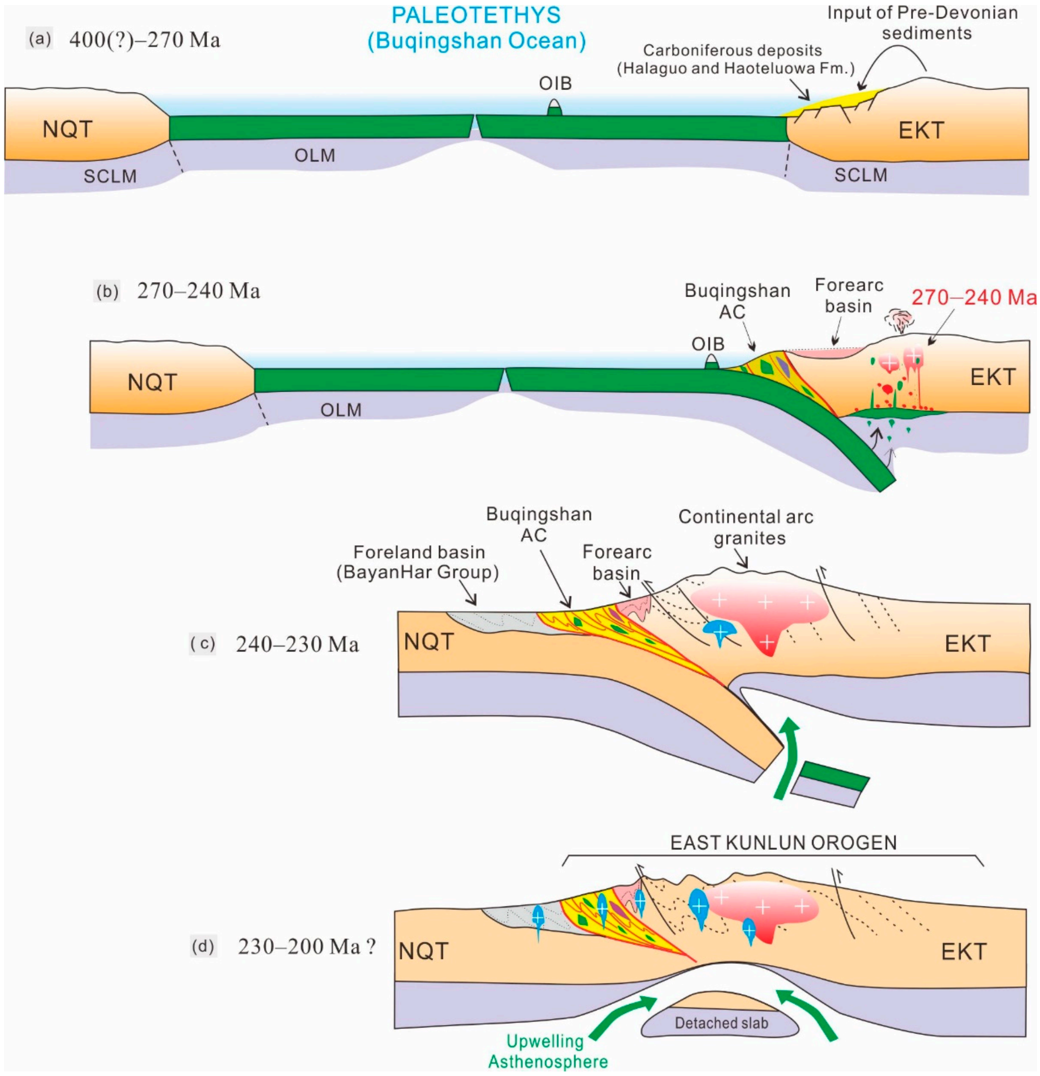

Figure 18. Cartoons showing the tectonic evolution of the Buqingshan Ocean during Late Paleozoic–Early Triassic time. (**a**) The spreading processes of Buqingshan Ocean, generating the OIBs and stable passive continental margin deposits in EKT; (**b**) subducting processes of Buqingshan Ocean, leading to the development of continental magmatic arc and forearc basin; (**c**) initial collision of the Qiangtang terrane with EKT showing the gradual tectonic emplacement of Buqingshan AC and production of minor collisional-type magmatism; (**d**) post-collisional stage showing the generation of A-type, high

Sr/Y granites and delamination processes of thickening lithosphere; NQT—North Qiangtang Terrane; BT—Bayan Har Terrane; EKT—East Kunlun Terrane; SCLM—Subcontinental lithospheric mantle; OLM—Oceanic lithospheric mantle. Red color with white cross shows continental arc magmatic rock, and blue color with white cross shows collisional-type magmatic rock.

6.1. Spreading of Buqingshan Ocean

Previous studies suggested that the development of the ocean in Kunlun can be subdivided into two stages: a Proto-Tethys from Late Neoproterozoic to Early Paleozoic time and a Paleo-Tethys from Late Paleozoic to Early Mesozoic time [12–14,20,23]. The two oceans are not temporally related, and consumption of the Proto-Tethys Ocean ultimately led to the formation of the pre-Devonian orogenic basement of the EKO [27,29,120]. Subsequently, the Paleo-Tethys Ocean gradually opened on the pre-Devonian orogenic basement of the EKO as early as the Devonian, although the opening timing and its transitional details from Proto-Tethys to Paleo-Tethys remain the subject of ongoing debate [4,12–14,20,23,120].

The existence of Early Carboniferous mantle peridotites, MORBs, and OIBs within Buqingshan AC indicates that an ocean was already open (Figures 5, 7 and 18a), thus the initial opening of the Buqingshan Ocean (BO) definitely predate the Early Carboniferous time. Moreover, Carboniferous siliciclastic–carbonate associations (Halaguole and Haoteluowa formations) and Lower to Middle Permian turbidites (Maerzheng Formation) in EKO were all deposited in a stable passive continental margin setting (Figure 4) [20,139,143]. In addition, there are few volcanic layers in the Carboniferous sequences in Eastern EKO. This further argues for a stable continental margin setting rather than a subduction-related setting in the Carboniferous.

From a global perspective, East Asia evolved to the Paleo-Tethys stage during the Late Paleozoic to Early Mesozoic [32,154–157]. During this time interval, several oceans opened across this region now represented by the Buqingshan, Jinsha, and Central Qiangtang oceans in the Tibet–Qinghai Plateau (Figure 19a) [32,51,158–160]. Further west, other approximately coeval oceans also developed in Tajikistan, NE Iran (Darrehanjir mélange), Turkey (Kure mélange), and the Caucasus [161,162]. These oceans were all branches of the Paleo-Tethys Ocean realm and constituted a complex ocean–continent configuration across parts of what is now Asia [32].

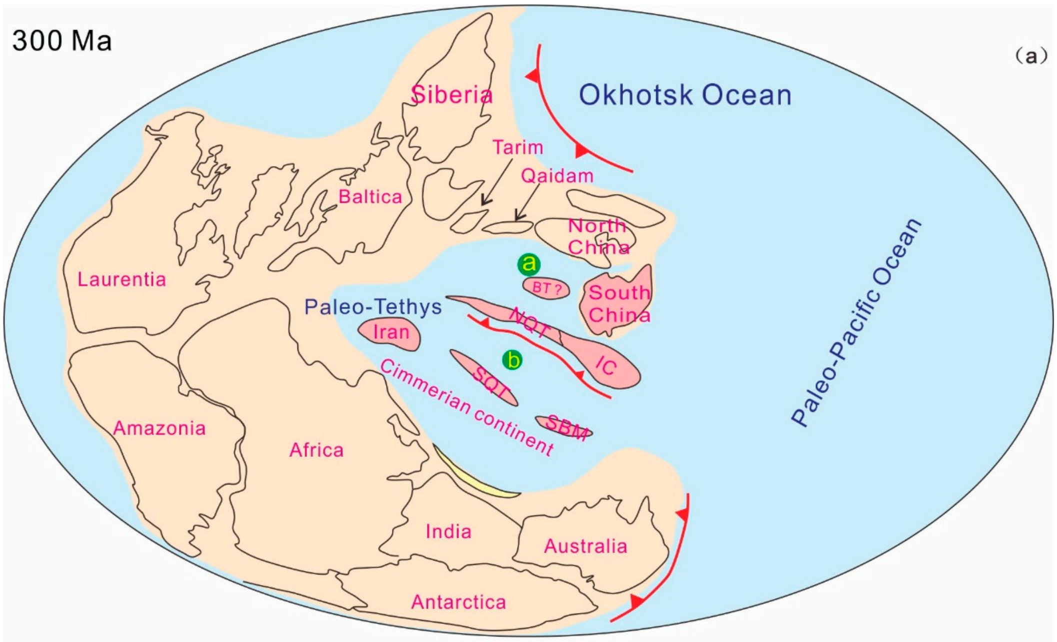

Figure 19. *Cont.*

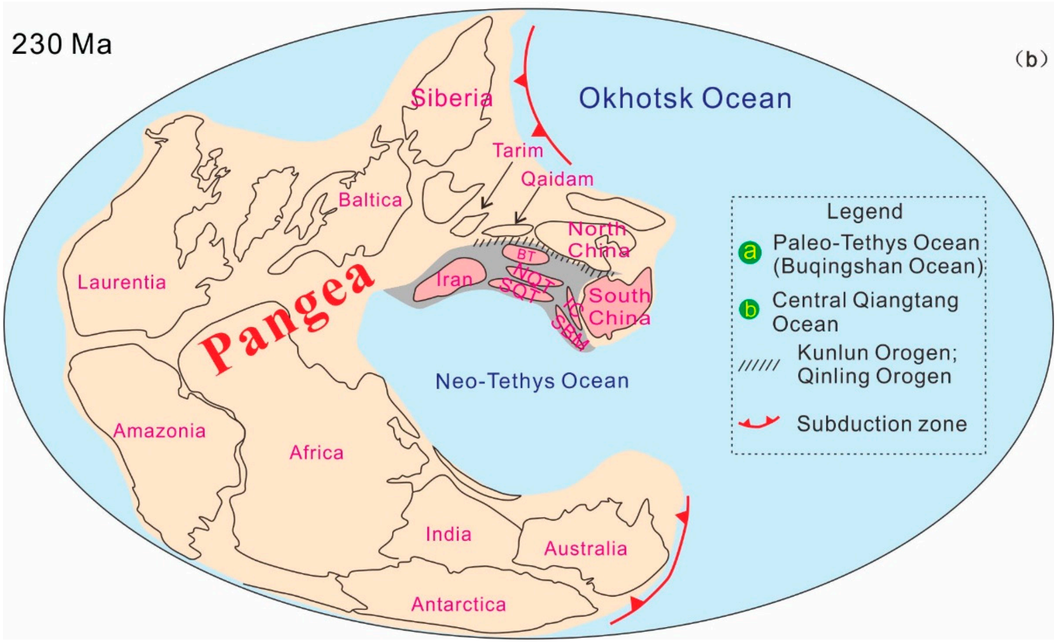

Figure 19. (**a**,**b**) Reconstruction of East Asian blocks showing the spreading and closure of Northern Paleo-Tethys Ocean (Buqingshan Ocean) (modified from the literature [32,52,157,163–165]). SQT—South Qiangtang Terrane; NQT—North Qiangtang Terrane; BT—Bayan Har terrane; SBM—Sibumasu Terrane; IC—Indochina Terrane.

6.2. Subduction of Buqingshan Ocean

During Late Permian to Middle Triassic time, the BO lithosphere was subducted beneath the EKT, leading to the development of Buqingshan AC, Burhan Budai continental arc magmatism, and forearc basin in EKO (Figure 18b). Two cross sections of Figure 6 across the Buqingshan AC showing top-to-the-south imbricated thrust faults and south-vergent tight-isoclinal asymmetrical folds suggest a north-dipping oceanic subduction zone associated with northward subduction of the Buqingshan Ocean. With the oceanic basin subducting northwards, the ocean island basalt together with the limestone were scraped and then accreted into the Buqingshan accretionary complex. Continued accretionary processes and tectonic deformation were accompanied by extensive greenschist facies metamorphism, which is marked by mineral associations of chlorites, epidotes, and sericites.

Meanwhile, the Hongshuichuan forearc basin formed between the Burhan Budai magmatic arc and Buqingshan AC (Figures 14, 17 and 18b). Detrital zircon age spectra clearly reveal that sediments of this basin were mainly sourced from the coeval continental magmatic arc to the north (Figures 14 and 16). This conclusion is further supported by the paleocurrent data of Yan et al. [144], which indicate sediment transportation predominantly to the SW. Liu [62] also reported that most sandstones from the lowermost part of the Hongshuichuan Formation plot within the “continental craton” provenance field of Dickinson [166], whereas the samples from the middle–upper part mainly plot within the “dissected arc” region, reflecting an upward increase in feldspar and lithic fragments and the contribution of detritus from the Burhan Budai magmatic arc.

In addition, south of the Paleo-Tethys Ocean, it likely diachronously subducted southward beneath the North Qiangtang terrane along the Jinshajiang tectonic zone. This is constrained by the occurrences of the Triassic Jinshajiang complex and island-arc granites along the northern margin of the North Qiangtang terrane [167–169]. We will not provide the details of the Jinshajiang tectonic zone as we mainly focus on the tectonics of EKO in this paper.

6.3. Syncollisional Stages of the BT with the Kunlun–Qaidam Terranes

Following the subduction and closure of the Buqingshan Ocean oblique collision of the Qiangtang terrane with the Kunlun–Qaidam terranes (KQT) occurred towards the end of the Middle Triassic (Figure 18c). This eventually led to the production of minor metaluminous–peraluminous granitoids, the emplacement of the Buqingshan AC, and the development of the Bayan Har peripheral foreland basin [61,170,171]. The closure of the Buqingshan Ocean is also marked by a regional angular unconformity between the Babaoshan Formation and the underlying marine successions [102,103]. This unconformity indicates that the northward subduction of the Paleo-Tethys Ocean lasted until the late Middle Triassic and that the collisional orogeny followed into the early Late Triassic. This collisional orogenesis produced the Kunlun and Qinling orogens in Central China (Figure 19b).

Regionally, the other branches (Jinsha, Central Qiangtang oceans, etc.), located on the SE Tibetan Plateau also closed, and eastern Cimmerian blocks collided to the north with the North Qiangtang/Bayan Har and South China blocks in the Late Triassic (Figure 19b) [157]. In a word, the closures of various branches of the Paleo-Tethys Ocean eventually led to the final formation of the East Asian continent during the Late Triassic (Figure 19b) [13,32,156,172].

6.4. Post-Collisional Stage

In the Late Triassic, the EKO evolved into a post-collisional collapse stage and produced major magmatic pulses (Figure 18d). The rate at which magma was added during the Late Triassic is estimated to have reached 100 km^3/m.y. [173,174], comparable to Late Mesozoic magmatic flare-up events from the central Sierra Nevada arc, California [175]. Tectono-magmatic events mainly include the generation of large volumes of adakitic granites and A-type granites, polymetallic mineral deposits, and MME-bearing granites, which are interpreted to be geodynamically related to asthenospheric mantle upwelling induced by delamination of thickened continental lithosphere and partial melting of the lower crust [47,130,176].

During the Early Jurassic, the EKO underwent rapid uplift and cooling as shown by zircon/apatite fission track data [177–183]. These events may have been induced by the unrooting of the over-thickened crust. The collapse of the over-thickened crust was accompanied by the generation of fault-bounded basins recorded by the Upper Triassic Babaoshan Formation (molasse deposits) and Lower Jurassic Yangqu Formation (coal-bearing strata).

7. Conclusions

A detailed synthesis of the petrological, sedimentary, geochemical, and isotopic features of the Late Paleozoic–Early Mesozoic geologic records from the EKO and adjacent regions leads to the following conclusions:

(1) The Buqingshan AC contains blocks of Carboniferous OIBs and MORBs, gabbros, depleted and refractory peridotites, and paleo-seamounts in a strongly deformed matrix of deep marine turbidites. The Buqingshan AC records the northward subduction of the Buqingshan Ocean from Late Paleozoic to the Middle Triassic time.

(2) Northward subduction of the Buqingshan Ocean beneath the Kunlun–Qaidam terrane led to the development of a vast continental magmatic arc (Burhan Budai arc) and the emplacement of seamounts into the Buqingshan AC around 270–240 Ma. During this interval, the Hongshuichuan forearc basin formed between the Burhan Budai arc and Buqingshan AC. Detrital zircon ages and paleocurrent data suggest most sedimentary detritus was supplied from the nearby Burhan Budai arc to the north with a minor contribution from an accretionary wedge to the south.

(3) Closure of the Buqingshan Ocean due to the collision of the Qiangtang terrane with East Kunlun terranes occurred during the late Middle Triassic to early Late Triassic (ca. 240–230 Ma) times. This led to the development of a regional angular unconformity between Upper Triassic terrigenous strata and underlying marine sediments.

(4) During the Late Triassic to Earliest Jurassic (ca. 230–200 Ma), the EKO evolved to a post-collisional stage that experienced magmatic flare-ups and metallic mineralization, which are interpreted to likely occur in geodynamic response to detachment of thickened lithosphere and subsequent upwelling of asthenosphere mantle.

Supplementary Materials: The following supporting information can be downloaded at: https://www.mdpi.com/article/10.3390/min12121590/s1, Table S1: The geochemical data for the mafic-ultramafic rocks in southern margin of EKO; Table S2: The geochemical data for continental arc- and collision-related magmatic rocks in EKO. References [18,27,50,61,63–65,71,81,84,89,91,109–122,124,139,147,149,152,183–192] are cited in the Supplementary Materials.

Author Contributions: Conceptualization, R.L. and X.P.; methodology, R.L.; software, R.L. and Z.L. (Zuochen Li); validation, R.L., X.P. and Z.L. (Zhanqing Liu); formal analysis, R.L. and X.P.; investigation, R.L., X.P., Z.L. (Zuochen Li), G.C., Y.C., L.P., C.L. and M.W.; resources, R.L. and X.P.; data curation, R.L. and X.P.; writing—original draft preparation, R.L. and X.P.; writing—review and editing, R.L., X.P. and M.Z.; visualization, R.L; supervision, R.L. and X.P.; project administration, R.L. and X.P.; funding acquisition, R.L. and X.P. All authors have read and agreed to the published version of the manuscript.

Funding: This research was jointly funded by the National Science Foundation of China (Grant Nos. 42172236, 41872233, 41502191, 41872235), National Science Foundation of Shaanxi Provence of China (Grant Nos. 2020JM-229), China Scholarship Council (Grant No, 201906565008), the Fundamental Research Funds for the Central Universities, CHD (Grant Nos. 300102279204), and the Youth Innovation Team of Shaanxi Universities.

Data Availability Statement: The original contributions presented in the study are included in the article/Supplementary Material.

Acknowledgments: Jonathan C. Aitchison and Goran Andjić are gratefully acknowledged for their comments and suggestions. Special thanks are extended to the chief editor and the two anonymous reviewers for their constructive reviews which have greatly improved our manuscript.

Conflicts of Interest: The authors declare no conflict of interest.

References

1. Harris, N.B.W.; Xu, R.; Lewis, C.L.; Jin, C. Plutonic rocks of the 1985 Tibet geotraverse, Lhasa to Golmud. *Philos. Trans. R. Soc. Lond. Ser. A* **1988**, *327*, 145–168.
2. Jiang, C.F. Opening-closing evolution of the Kunlun Mountains. Opening closing tectonics of Kunlun Shan. *Geol. Memo* **1992**, *5*, 205–217. (In Chinese with English Abstract)
3. Bian, Q.T.; Luo, X.Q.; Li, H.S.; Chen, H.H.; Zhao, D.S. Discovery of Early Paleozoic and Early Carboniferous-Early Permian ophiolites in the A'nyemaqen, Qinghai Province, China. *Sci. Geol. Sin.* **1999**, *34*, 523–524. (In Chinese with English Abstract)
4. Bian, Q.T.; Li, D.H.; Pospelov, I.; Yin, L.M.; Li, H.S.; Zhao, D.S.; Chang, C.F.; Luo, X.Q.; Gao, S.L.; Astrakhantsev, O.; et al. Age, geochemistry and tectonic setting of Buqingshan ophiolites, North Tibet Plateau, China. *J. Asian Earth Sci.* **2004**, *23*, 577–596. [CrossRef]
5. Yang, J.S.; Robison, P.T.; Jiang, C.F.; Xu, Z.Q. Ophiolites of the Kunlun Mountains, China and their tectonic implications. *Tectonophysics* **1996**, *258*, 215–231. [CrossRef]
6. Yang, J.S.; Xu, Z.Q.; Ma, C.Q.; Wu, C.L.; Zhang, J.X.; Wang, Z.Q.; Wang, G.C.; Zhang, H.F.; Dong, Y.P.; Lai, S.C. Compound orogeny and scientific problems concerning the Central Orogenic Belt of China. *Geol. China* **2010**, *37*, 1–11. (In Chinese with English Abstract)
7. Wang, G.C.; Zhang, T.P.; Liang, B.; Chen, N.S.; Zhu, Y.H.; Zhu, J. Composite ophiolite melange zone in central part of eastern section of East Kunlun Orogen and geological significance of 'Fault belt in central part of eastern section of East Kunlun Orogen. *Earth Sci.* **1999**, *24*, 129–133.
8. Yin, A.; Harrison, T.M. Geologic evolution of the Himalayan-Tibetan orogeny. *Annu. Rev. Earth Planet. Sci.* **2000**, *28*, 211–280. [CrossRef]
9. Zhang, J.X.; Yang, J.S.; Meng, F.C.; Wan, Y.S.; Li, H.M.; Wu, C.L. U-Pb isotopic studies of eclogites and their host gneisses in the Xitieshan area of the North Qaidam mountains, western China: New evidence for an early Paleozoic HP-UHP metamorphic belt. *J. Asian Earth Sci.* **2006**, *28*, 143–150.
10. Mo, X.X.; Luo, Z.H.; Deng, J.F.; Yu, X.H.; Liu, C.D.; Chen, H.W.; Yuan, W.M.; Liu, Y.H. Granitoids and crustal growth in the East Kunlun Orogenic Belt. *Geol. J. China Univ.* **2007**, *13*, 403–414. (In Chinese with English Abstract)

11. Xu, Z.Q.; Yang, J.S.; Li, W.C.; Li, Q.H.; Cai, Z.H.; Yan, Z.; Ma, C.Q. Paleo-Tethys system and accretionary orogen in the Tibet Plateau. *Acta Petrol. Sin.* **2013**, *29*, 1847–1860. (In Chinese with English Abstract)
12. Dong, Y.P.; He, D.F.; Sun, S.S.; Liu, X.M.; Zhou, X.H.; Zhang, F.F.; Yang, Z.; Cheng, B.; Zhao, G.C.; Li, J.H. Subduction and accretionary tectonics of the East Kunlun orogen, western segment of the Central China Orogenic System. *Earth-Sci. Rev.* **2018**, *186*, 231–261. [CrossRef]
13. Dong, Y.P.; Sun, S.S.; Santosh, M.; Zhao, J.; Sun, J.P.; He, D.F.; Shi, X.H.; Hui, B.; Cheng, C.; Zhang, G.W. Central China Orogenic Belt and amalgamation of East Asian continents. *Gondwana Res.* **2021**, *100*, 131–194. [CrossRef]
14. Pei, X.Z.; Li, R.B.; Li, Z.C.; Liu, C.J.; Chen, Y.X.; Pei, L.; Liu, Z.Q.; Chen, G.C.; Li, X.B.; Wang, M. Composition Feature and Formation Process of Buqingshan Composite Accretionary Mélange Belt in Southern Margin of East Kunlun Orogen. *Earth Sci.* **2018**, *43*, 4498–4520. (In Chinese with English Abstract)
15. Peng, Y.B.; Yu, S.Y.; Li, S.Z.; Zhang, J.X.; Liu, Y.J. Early Neoproterozoic magmatic imprints in the Altun-Qilian-Kunlun region of the Qinghai-Tibet Plateau: Response to the assembly and breakup of Rodinia supercontinent. *Earth-Sci. Rev.* **2019**, *199*, 102954. [CrossRef]
16. Leeder, M.R.; Smith, A.B.; Yin, J. Sedimentology, palaeoecology and palaeoenvironmental evolution of the 1985 Lhasa to Golmud Geotraverse. *Philos. Trans. R. Soc. Lond. Ser. A* **1988**, *327*, 107–143.
17. Matte, P. Tectonics of western Tibet, between the Tarim and the Indus, Earth Planet. *Sci. Lett.* **1996**, *142*, 311–330.
18. Liu, B.; Ma, C.Q.; Zhang, J.Y.; Xiong, F.H. 40Ar–39Ar age and geochemistry of subductionrelated mafic dikes in northern Tibet, China:petrogenesis and tectonic implications. *Int. Geol. Rev.* **2014**, *56*, 57–73. [CrossRef]
19. Meng, F.C.; Zhang, J.X.; Cui, M. Discovery of Early Paleozoic eclogite from the East Kunlun, Western China and its tectonic significance. *Gondwana Res.* **2013**, *23*, 825–836. [CrossRef]
20. Wu, C.; Zuza, A.V.; Zhou, Z.G.; Yin, A.; McRivette, M.W.; Chen, X.H.; Ding, L.; Geng, J.Z. Mesozoic-Cenozoic evolution of the Eastern Kunlun Range, central Tibet, and implications for basin evolution during the Indo-Asian collision. *Lithosphere* **2019**, *11*, 524–550. [CrossRef]
21. Yan, Z.; Fu, C.L.; Aitchison, J.C.; Buckman, S.; Niu, M.L.; Cao, B. Triassic turbidites in the West Qinling Mountains, NW China: Part of the collisional Songpan-Ganzi Basin or an active forearc basin? *J. Asian Earth Sci.* **2020**, *194*, 104366. [CrossRef]
22. Yu, M.; Dick, J.M.; Feng, C.Y.; Li, B.; Wang, H. The tectonic evolution of the East Kunlun Orogen, northern Tibetan Plateau: A critical review with an integrated geodynamic model. *J. Asian Earth Sci.* **2020**, *191*, 104–168. [CrossRef]
23. Yu, S.Y.; Li, S.Z.; Zhang, J.X.; Peng, Y.B.; Somerville, I.; Liu, Y.J.; Wang, Z.Y.; Li, Z.F.; Yao, Y.; Li, Y. Multi-stage anatexis during tectonic evolution from oceanic subduction to continental collision: A review of the North Qaidam UHP Belt, NW China. *Earth-Sci. Rev.* **2019**, *191*, 190–211. [CrossRef]
24. Chen, N.S.; He, L.; Wang, G.C.; Zhang, K.X.; Sun, M. Precise age definition of early Paleozoic peak metamorphism and thrust tectonic deformation in East Kunlun Orogenic Belt. *Chin. Sci. Bull.* **2002**, *47*, 628–631. (In Chinese with English Abstract)
25. Li, R.B.; Pei, X.Z.; Pei, L.; Li, Z.C.; Sun, Y.; Pei, L.; Chen, G.C.; Chen, Y.X. Regional Tectonic Transformation in East Kunlun Orogenic Belt in Early Paleozoic: Constraints from the Geochronology and Geochemistry of Helegangnaren Alkali-feldspar Granite. *Acta Geol. Sin.* **2013**, *87*, 333–345.
26. Qi, S.S.; Song, S.G.; Shi, L.C.; Cai, H.J.; Hu, J.C. Discovery and its geological significance of Early Paleozoic eclogite in Xiarihamu-Suhaitu area, western part of the East Kunlun. *Acta Petrol. Sin.* **2014**, *30*, 3345–3356. (In Chinese with English Abstract)
27. Xiong, F.H.; Ma, C.Q.; Jiang, H.A.; Liu, B.; Huang, J. Geochronology and geochemistry of middle Devonian mafic dykes in the East Kunlun orogenic belt, northern Tibet plateau: Implications for the transition from Prototethys to Paleotethys orogeny. *Chem. Der Erde-Geochem.* **2014**, *74*, 225–235. [CrossRef]
28. Xiong, F.; Ma, C.; Zhang, J.; Liu, B.; Jiang, H. Reworking of old continental lithosphere: An important crustal evolution mechanism in orogenic belts, as evidenced by Triassic I-type granitoids in the East Kunlun orogen, Northern Tibetan Plateau. *J. Geol. Soc. Lond.* **2014**, *171*, 847–863. [CrossRef]
29. Li, S.; Zhao, S.; Liu, X.; Cao, H.; Yu, S.; Li, X.; Somerville, I.; Yu, S.; Suo, Y. Closure of the Proto-Tethys Ocean and Early Paleozoic amalgamation of microcontinental blocks in East Asia. *Earth-Sci. Rev.* **2018**, *186*, 37–75. [CrossRef]
30. Xin, W.; Sun, F.Y.; Li, L.; Yan, J.M.; Zhang, Y.T.; Wang, Y.C.; Shen, T.S.; Yang, Y.J. The Wulonggou metaluminous A2-type granites in the eastern Kunlun orogenic belt, NW China: Rejuvenation of subduction-related felsic crust and implications for post-collision extension. *Lithos* **2018**, *312–313*, 108–127. [CrossRef]
31. Li, W.Y.; Zhang, Z.W.; Wang, Y.L.; Zhang, J.W.; You, M.X.; Zhang, Z.B. Tectonic transformation of Proto- and Paleo-Tethys and the mineralization of magmatic Ni-Cu-Co sulphide deposites in Kunlun Orogen, Northwest China. *J. Earth Sci. Eviron.* **2022**, *44*, 1–19. (In Chinese with English Abstract)
32. Zhao, G.; Wang, Y.; Huang, B.; Dong, Y.; Li, S.; Zhang, G.; Yu, S. Geological reconstructions of the East Asian blocks: From the breakup of Rodinia to the assembly of Pangea. *Earth-Sci. Rev.* **2018**, *186*, 262–286. [CrossRef]
33. Pei, X.Z. Geological Evolution and Dynamics of the Mianlue-A'nimaqen Tectonic Zone, Central China. Ph.D. Thesis, Northwest University, Singapore, 2001; pp. 1–61.
34. Pei, X.Z.; Zhang, G.W.; Lai, S.C.; Li, Y.; Chen, L.; Gao, M. Main geological features of the Mianlue tectonic belt on the southern margin of the West Qinling. *Geol. Bull. China* **2002**, *21*, 486–494. (In Chinese with English Abstract)
35. Dong, Y.P.; Liu, X.M.; Neubauer, F.; Zhang, G.W.; Tao, N.; Zhang, Y.G. Timing of Paleozoic amalgamation between the North China and South China Blocks: Evidence from detrital zircon U-Pb ages. *Tectonophysics* **2013**, *586*, 173–191. [CrossRef]

36. Dong, Y.P.; Santosh, M. Tectonic architecture and multiple orogeny of the Qinling Orogenic Belt, Central China. *Gondwana Res.* **2016**, *29*, 1–40. [CrossRef]
37. Dong, Y.P.; Sun, S.S.; Liu, X.M.; He, D.F.; Zhou, X.H.; Zhang, F.F.; Yang, Z.; Zhou, D.W. Geochronology and geochemistry of the Yazidaban ophiolitic mélange in Qimantagh: Contraints on the Early Paleozoic back-arc basin of the East Kunlun Orogen, northern Tibetan Plateau. *J. Geol. Soc. Lond.* **2019**, *176*, 306–322. [CrossRef]
38. Hou, G.J.; Wang, G.C.; Zhang, K.X.; Chen, N.S.; Zhu, Y.H.; Bai, Y.S. Superimposed folds and corresponding deformation mechanism in foreland basins in Eastern Kunlun Orogenic Zone. *Earth Sci.* **1999**, *24*, 125–128. (In Chinese with English Abstract)
39. Yin, H.F.; Zhang, K.X.; Chen, N.S. *Regional Geological Report of the People's Republic of China: Map of Dongjicuonahe Region (No, I47C001002) at Scale: 1:250,000*; China University of Geoscience Press: Wuhan, China, 2003.
40. Huang, H.; Niu, Y.; Nowell, G.; Zhao, Z.; Yu, X.; Zhu, D.C.; Mo, X.; Ding, S. Geochemical constraints on the petrogenesis of granitoids in the East Kunlun Orogenic belt, northern Tibetan Plateau: Implications for continental crust growth through syn-collisional felsic magmatism. *Chem. Geol.* **2014**, *370*, 1–18. [CrossRef]
41. Li, R.S.; Chen, J.L.; Ma, Z.P.; Xu, X.Y.; Zha, X.F.; Bai, J.K.; Shi, C.; Zhang, H.D. Recognition and confirmation of Paleozoic accretionary wedges in Subducted orogenic zone, Northwest China. *Geol. Surv. China* **2016**, *3*, 44–51.
42. Kong, J.; Niu, Y.; Hu, Y.; Zhang, Y.; Shao, F. Petrogenesis of the Triassic granitoids from the East Kunlun Orogenic Belt, NW China: Implications for continental crust growth from syn-collisional to post-collisional setting. *Lithos* **2020**, *364–365*, 105513. [CrossRef]
43. Jiang, Y.H.; Jia, R.Y.; Liu, Z.; Liao, S.Y.; Zhao, P.; Zhou, Q. Origin of Middle Triassic high-K calc-alkaline granitoids and their potassic microgranular enclaves from the west Kunlun orogen, northwest China: A record of the closure of Paleo-Tethys. *Lithos* **2013**, *156–159*, 13–30. [CrossRef]
44. Chen, G.C.; Pei, X.Z.; Li, R.B.; Li, Z.C.; Pei, L.; Liu, Z.Q.; Chen, Y.X.; Liu, C.J.; Gao, J.M.; Wei, F.H. Zircon U-Pb geochronology, geochemical characteristics and geological significance of Cocoe A'Long quartz diorites body from the Hongshuichuan Area in East Kunlun. *Acta Geol. Sin.* **2013**, *87*, 178–196. (In Chinese with English Abstract)
45. Chen, G.C.; Pei, X.Z.; Li, R.B.; Li, Z.C.; Liu, C.J.; Chen, Y.X.; Pei, L.; Li, X.B. Age and lithogenesis of Keri syenogranite from eastern part of East Kunlun Orogenic Belt: Constraint on the Middle Triassic tectonic evolution of East Kunlun. *Acta Petrol. Sin.* **2018**, *34*, 567–585. (In Chinese with English Abstract)
46. Chen, G.C.; Pei, X.Z.; Li, R.B.; Li, Z.C.; Pei, L.; Liu, C.J.; Chen, Y.X.; Wang, M.; Zhang, Y.; Li, X.B. Magma mixing in Halagatu granitic batholith from eastern part of the East Kunlun Orogenic Belt: Constraints from lithology and mineralogy. *Earth Sci.* **2018**, *43*, 3200–3217. (In Chinese with English Abstract)
47. Chen, G.C.; Pei, X.Z.; Li, R.B.; Li, Z.C.; Pei, L.; Liu, C.J.; Chen, Y.X.; Wang, M.; Gao, F.; Li, X.B. Lithospheric extension of the post-collision stage of the Paleo-Tethys oceanic system in the East Kunlun Orogenic Belt: Insights from Late Triassic plutons. *Earth-Sci. Front.* **2019**, *26*, 191–208. (In Chinese with English Abstract) [CrossRef]
48. Chen, G.C.; Pei, X.Z.; Li, R.B.; Li, Z.C.; Liu, C.J.; Chen, Y.X.; Wang, M.; Gao, F.; Wei, J.Q. Late Paleozoic-Early Mesozoic tectonic-magmatic evolution and mineralization in the eastern section of East Kunlun Orogenic Belt. *Earth-Sci. Front.* **2020**, *27*, 33–48.
49. Li, R.B.; Pei, X.Z.; Pei, L.; Li, Z.C.; Chen, G.C.; Chen, Y.X.; Liu, C.J.; Wang, M. The Early Triassic Andean-type Halagatu granitoids pluton in the East Kunlun orogen, northern Tibet Plateau: Response to the northward subduction of the Paleo-Tethys Ocean. *Gondwana Res.* **2018**, *62*, 212–226. [CrossRef]
50. Li, R.B.; Pei, X.Z.; Li, Z.C.; Pei, L.; Chen, G.C.; Chen, Y.X.; Liu, C.J.; Wang, S.M. Paleo-Tethys Ocean subduction in eastern section of East Kunlun Orogen: Evidence from the geochronology and geochemistry of the Wutuo pluton. *Acta Petrol. Sin.* **2018**, *34*, 3399–3421. (In Chinese with English Abstract)
51. Roger, F.; Arnaud, N.; Gilder, S.; Tapponnier, P.; Jolivet, M.; Brunel, M.; Malavieille, J.; Xu, Z.Q.; Yang, J.S. Geochronological and geochemical constraints on Mesozoic suturing in east central Tibet. *Tectonics* **2003**, *22*, 1037. [CrossRef]
52. Zuza, A.V.; Yin, A. Balkatach hypothesis: A new model for the evolution of the Pacific, Tethyan, and Paleo-Asian oceanic domains. *Geosphere* **2017**, *13*, 1664–1712. [CrossRef]
53. Zhang, J.; Yang, Z.; Zhang, H.; Ma, C.; Li, J.; Pan, Y. Controls on the formation of Cu-rich magmas: Insights from the Late Triassic post-collisional Saishitang complex in the eastern Kunlun Orogen, western China. *Lithos* **2017**, *278–281*, 400–418. [CrossRef]
54. Xiong, F.; Ma, C.; Jiang, H.a.; Zhang, H. Geochronology and petrogenesis of Triassic high-K calc-alkaline granodiorites in the East Kunlun orogen, West China: Juvenile lower crustal melting during post-collisional extension. *J. Earth Sci.* **2016**, *27*, 474–490. [CrossRef]
55. Zhang, Y.; Niu, Y.; Hu, Y.; Liu, J.; Ye, L.; Kong, J.; Duan, M. The syncollisional granitoid magmatism and continental crust growth in the West Kunlun Orogen, China—Evidence from geochronology and geochemistry of the Arkarz pluton. *Lithos* **2016**, *245*, 191–204. [CrossRef]
56. Li, B.; Zhi, Y.; Zhang, L.; Ding, Q.; Xu, Q.; Zhang, Y.; Qian, Y.; Wang, G.; Peng, B.; Ao, C. U-Pb dating, geochemistry, and Sr-Nd isotopic composition of a granodiorite porphyry from the Jiadanggen Cu-(Mo) deposit in the Eastern Kunlun metallogenic belt, Qinghai Province, China. *Ore. Geol. Rev.* **2015**, *67*, 1–10. [CrossRef]
57. Chen, X.H.; Yin, A.; Gehrels, G.; Li, L.; Jiang, R.B. Chemical Geodynamics of granitic magmatism in the basement of the Eastern Qaidam Basin, Northern Qinghai-Tibet Plateau. *Acta Geol. Sin.* **2011**, *85*, 157–171. (In Chinese with English Abstract)
58. Li, X.; Huang, X.; Luo, M.; Dong, G.; Mo, X. Petrogenesis and geodynamic implications of the Mid-Triassic lavas from East Kunlun, northern Tibetan Plateau. *J. Asian Earth Sci.* **2015**, *105*, 32–47. [CrossRef]

59. Shao, F.; Niu, Y.; Liu, Y.; Chen, S.; Kong, J.; Duan, M. Petrogenesis of Triassic granitoids in the East Kunlun Orogenic Belt, northern Tibetan Plateau and their tectonic implications. *Lithos* **2017**, *282–283*, 33–44. [CrossRef]
60. Li, B.L.; Sun, F.Y.; Yu, X.F.; Qian, Y.; Wang, G.; Yang, Y.Q. U-Pb dating and geochemistry of diorite in the eastern section from Eastern Kunlun middle uplifted basement and granitic belt. *Acta Petrol. Sin.* **2012**, *28*, 1163–1172. (In Chinese with English Abstract)
61. Li, Z.C.; Pei, X.Z.; Liu, Z.Q.; Li, R.B.; Pei, L.; Chen, G.C.; Liu, C.J.; Chen, Y.X.; Gao, J.M.; Wei, F.H.; et al. Geochronology and geochemistry of the Gerizhuotuo diorites from the Buqingshan Tectonic Mélange Belt in the southern margin of East Kunlun and Their geologic implications. *Acta Geol. Sin.* **2013**, *87*, 1089–1103. (In Chinese with English Abstract)
62. Liu, T.J. Geologic Features, Provenance Nature and Tectonic Significance of Hongshuichuan Formation Located in the Southern Slope of the East Kunlun Orogenic Belt (Eastern Part). Master's Thesis, Chang'an University, Xi'an, China, 2015.
63. Li, P. Geological Characteristics, Genesis and Geological Significance of Indosinian Granitic Pluton in Bolositai Region, East Section of East Kunlun Orogenic Belt. Master's Thesis, Chang'an University, Xi'an, China, 2019. (In Chinese with English Abstract).
64. Xiong, F.H.; Ma, C.Q.; Zhang, J.Y.; Liu, B. The origin of mafic microgranular enclaves and their host granodiorites from East Kunlun, Northern Qinghai-Tibet Plateau: Implications for magma mixing during subduction of Paleo-Tethyan lithosphere. *Mineral. Petrol.* **2011**, *104*, 211–224. [CrossRef]
65. Ding, S.; Huang, H.; Niu, Y.L.; Zhao, Z.D.; Yu, X.H.; Mo, X.X. Geochemistry, geochronology and petrogenesis of East Kunlun high Nb-Ta rhyolites. *Acta Petrol. Sin.* **2011**, *27*, 3603–3614. (In Chinese with English Abstract)
66. Liu, J.N.; Feng, C.Y.; Qi, F.; Li, G.C.; Ma, S.C.; Xiao, Y. SIMS zircon U-Pb dating and fluid inclusion studies of Xiadeboli Cu-Mo ore district in Dulan County, Qinghai Province, China. *Acta Petrol. Sin.* **2012**, *28*, 679–690. (In Chinese with English Abstract)
67. Deng, H.B.; He, L.; Yao, B.; Guan, Y.B.; Tang, H. Formation age and geochemical characteristics of Dishantou Monzonitic granite in Eastern Kunlun Orogenic Belt. *Northwest. Geol.* **2018**, *51*, 60–69. (In Chinese with English Abstract)
68. Wei, X.L.; Zeng, X.P.; Gan, C.P.; Zhang, D.P.X.; Yu, X.L. Geochemistry and Geological Significance of Intermediate-Acid Intrusive Rocks in Chaganganuo Area, East Kunlun. *Northwest. Geol.* **2016**, *49*, 1–10. (In Chinese with English Abstract)
69. Chang, Y.Y.; Li, J.F.; Zhang, J.; Cao, S.X.; Li, P.P.; Chen., H.Q. Study of environment and chronology of Late Triassic intrusive rocks in East Nalinggele River of Qinghai. *Northwest. Geol.* **2009**, *42*, 57–65. (In Chinese with English Abstract)
70. Wang, S.; Feng, C.Y.; Li, S.J.; Jiang, J.H.; Li, D.S.; Su, S.S. Zircon SHRIMP U-Pb dating of granodiorite in the Kaerqueka polymetallic ore deposit, Qimatag Mountain, Qinghai Province, and its geological implications. *Geol. China* **2009**, *36*, 74–84. (In Chinese with English Abstract)
71. Feng, C.Y.; Wang, S.; Li, G.C.; Ma, S.C.; Li, D.S. Middle to Late Triassic granitoids in the Qimatag area, Qinghai Province, China: Chronology, geochemistry and metalogenic significances. *Acta Petrol. Sin.* **2012**, *28*, 665–678. (In Chinese with English Abstract)
72. Wang, B.Z.; Luo, Z.H.; Li, H.Y.; Chen, H.W.; Hu, X.L. Petrotectonic assemblages and temporal-spatial framework of the Late Paleozoic-Early Mesozoic intrusions in the Qimatag Corridor of the East Kunlun belt. *Geol. China* **2009**, *36*, 769–782. (In Chinese with English Abstract)
73. Li, S.J.; Sun, F.Y.; Feng, C.Y.; Liu, Z.H.; Zhao, J.W.; Li, Y.C.; Wang, S. Geochronological study on Yazigou polymetallic deposit in Eastern Kunlun, Qinhai Province. *Acta Geol. Sin.* **2008**, *82*, 949–955. (In Chinese with English Abstract)
74. Xi, R.G.; Xiao, P.X.; Wu, Y.Z.; Dong, Z.C.; Guo, L.; Gao, X.F. The geological significances, composition and age of the Monzonitic granite in Kendekeke iron mine. *Northwest. Geol.* **2010**, *43*, 195–202. (In Chinese with English Abstract)
75. Wu, X.K.; Meng, F.C.; Xu, H.; Cui, M.H. Zircon U-Pb dating, geochemistry and Nd-Hf isotopic compositions of the Maxingdaban Late Triassic granitic pluton from Qimatagh in the Eastern Kunlun. *Acta Petrol. Sin.* **2011**, *27*, 3380–3394. (In Chinese with English Abstract)
76. Zhang, G. Research on Geological Characteristics, Ages and Geological Significance of the Halagatu Granitic Rocks in East Segment of the East Kunlun Orogen. Master's Thesis, Chang'an University, Xi'an, China, 2012. (In Chinese with English Abstract).
77. Sun, Y.; Pei, X.Z.; Ding, S.P.; Li, R.B.; Feng, J.Y.; Zhang, Y.F.; Li, Z.C.; Chen, Y.X.; Zhang, X.F.; Chen, G.H. Halagatu magma mixing granite in the East Kunlun Mountains-evidence from Zircon U-Pb dating. *Acta Geol. Sin.* **2009**, *83*, 1000–1010. (In Chinese with English Abstract)
78. Liu, C.D.; Mo, X.X.; Luo, Z.H.; Yu, X.H.; Chen, H.W.; Li, S.W.; Zhao, X. Crust-mantle magmatism of the Eastern Kunlun: Evidence from zircon SHRIMP dating. *Sci. Bull.* **2004**, *49*, 596–602. (In Chinese with English Abstract)
79. Li, Z.; Pei, X.; Li, R.; Pei, L.; Chen, Y.; Liu, C.; Liu, Z.; Chen, G.; Wang, M.; Zhao, S. The latest tectonic magmatism in the Buqingshan-A'nyemaqen tectonic mélange belt: Evidence from zircon U-Pb geochronology of intermediate-basic dikes, northern Tibetan Plateau, China. *Arab. J. Geosci.* **2019**, *12*, 374. [CrossRef]
80. Zhao, X.; Fu, L.; Wei, J.; Bagas, L.; Santosh, M.; Liu, Y.; Zhang, D.; Zhou, H. Late Permian back-arc extension of the eastern Paleo-Tethys Ocean: Evidence from the East Kunlun Orogen, Northern Tibetan Plateau. *Lithos* **2019**, *340–341*, 34–48. [CrossRef]
81. Kong, H.L.; Li, J.C.; Li, Y.Z.; Jia, Q.Z.; Guo, X.Z.; Zhang, B. Zircon U-Pb dating and geochemistry of the Jiadang olivine gabbro in the eastern section of East Kunlun, Qinghai Province and their geological significance. *Acta Geol. Sin.* **2018**, *92*, 964–979. (In Chinese with English Abstract)
82. Zhang, M.D.; Ma, C.Q.; Wang, L.X.; Hao, F.H.; Zheng, S.J.; Zhang, L. Subduction-type magmatic rocks in post-collision stage: Evidence from Late Triassic diorite-porphyrite of Naomuhun area, East Kunlun Orogen. *Earth Sci.* **2018**, *43*, 1183–1206. (In Chinese with English Abstract)

83. Xue, H.R.; Sun, F.Y.; Li, L.; Xin, W. Geochronology, geochemistry, and Sr-Nd-Hf isotopes of the Late Permian-Early Triassic granitoids in Eastern Kunlun Orogen, Northwest China: Petrogenesis and implications for geodynamic setting. *Int. Geol. Rev.* **2020**, *63*, 696–716. [CrossRef]
84. Xiong, F.; Ma, C.; Chen, B.; Ducea, M.N.; Hou, M.; Ni, S. Intermediate-mafic dikes in the East Kunlun Orogen, northern Tibetan Plateau: A window into paleo-arc magma feeding system. *Lithos* **2019**, *340–341*, 152–165. [CrossRef]
85. Xin, W.; Sun, F.Y.; Zhang, Y.T.; Fan, X.Z.; Wang, Y.C.; Li, L. Mafic-intermediate igneous rocks in the East Kunlun Orogenic Belt, northwestern China: Petrogenesis and implications for regional geodynamic evolution during the Triassic. *Lithos* **2019**, *346–347*, 105–159. [CrossRef]
86. Song, K.; Ding, Q.F.; Zhang, Q.; Cheng, L.; Han, Y.; Liu, F.; Liu, Y. Zircon U-Pb geochronology, Hf isotopes, and whole-rock geochemistry of Hongshuihe Early to Middle Triassic quartz diorites and granites in the Eastern Kunlun Orogen, NW China: Implication for petrogenesis and geodynamics. *Geol. J.* **2019**, *63*, 696–716. [CrossRef]
87. Yao, L.; Dong, S.Y.; Lü, Z.C.; Zhao, C.S.; Pang, Z.S.; Yu, X.F.; Xue, J.L.; Geng, L.; Zhang, Z.H.; Liu, Y. Origin of the Late Permian gabbros and Middle Triassic granodiorites and their mafic microgranular enclaves from the Eastern Kunlun Orogen Belt: Implications for the subduction of the Paleo-Tethys Ocean and continent-continent collision. *Geol. J.* **2018**, *55*, 147–172. [CrossRef]
88. Chen, J.; Wei, J.; Fu, L.; Li, H.; Zhou, H.; Zhao, X.; Zhan, X.; Tan, J. Multiple sources of the Early Mesozoic Gouli batholith, Eastern Kunlun Orogenic Belt, northern Tibetan Plateau: Linking continental crustal growth with oceanic subduction. *Lithos* **2017**, *292–293*, 161–178. [CrossRef]
89. Ding, Q.F.; Liu, F.; Yan, W.; Li, B.; Sun, F. Zircon U-Pb geochronology and Hf isotopic constraints on the petrogenesis of Early Triassic granites in the Wulonggou area of the Eastern Kunlun Orogen, Northwest China. *Int. Geol. Rev.* **2015**, *57*, 1735–1754. [CrossRef]
90. Xia, R.; Wang, C.; Deng, J.; Carranza, E.J.M.; Li, W.; Qing, M. Crustal thickening prior to 220Ma in the East Kunlun Orogenic Belt: Insights from the Late Triassic granitoids in the Xiao-Nuomuhong pluton. *J. Asian Earth Sci.* **2014**, *93*, 193–210. [CrossRef]
91. Shi, L.C.; Chang, G.H.; Qi, S.S.; Chen, G.T.; Zhao, M.F.; Xu, B. The discovery of Dazaohuogou-Wanbaogou Late Permian epicontinental arc volcanic rocks in Eastern Kunlun Mountains and its significance. *Geol. Bull. China* **2016**, *35*, 1115–1122. (In Chinese with English Abstract)
92. Yuan, C.; Sun, M.; Xiao, W.; Wilde, S.; Li, X.; Liu, X.; Long, X.; Xia, X.; Ye, K.; Li, J. Garnet-bearing tonalitic porphyry from East Kunlun, Northeast Tibetan Plateau: Implications for adakite and magmas from the MASH Zone. *Int. J. Earth Sci.* **2008**, *98*, 1489–1510. [CrossRef]
93. Liu, Y.; Genser, J.; Neubauer, F.; Jin, W.; Ge, X.; Handler, R.; Takasu, A. 40Ar/39Ar mineral ages from basement rocks in the Eastern Kunlun Mountains, NW China, and their tectonic implications. *Tectonophysics* **2005**, *398*, 199–224. [CrossRef]
94. Chen, Y.X.; Pei, X.Z.; Li, R.B.; Li, Z.C.; Pei, L.; Liu, Z.Q.; Chen, G.C.; Liu, C.J.; Yang, J. Association, geochemical characteristics and tectonic setting of the Xiaomiao Formation, east region of East Kunlun Orogenic Belt. *Acta Geol. Sin.* **2014**, *88*, 1038–1054. (In Chinese with English Abstract)
95. Chen, Y.X.; Pei, X.Z.; Li, R.B.; Liu, Z.Q.; Li, Z.C.; Zhang, X.F.; Chen, G.C.; Liu, Z.G.; Ding, S.P.; Guo, J.F. Zircon U-Pb age of Xiaomiao Formation of Proterozoic in the eastern section of the East Kunlun Orogenic Belt. *Geoscience* **2011**, *25*, 510–521. (In Chinese with English Abstract)
96. He, D.; Dong, Y.; Liu, X.; Yang, Z.; Sun, S.; Cheng, B.; Li, W. Tectono-thermal events in East Kunlun, Northern Tibetan Plateau: Evidence from zircon U-Pb geochronology. *Gondwana Res.* **2016**, *30*, 179–190. [CrossRef]
97. Zhang, Q.; Ding, Q.F.; Song, K.; Cheng, L. Detrital Zircon U-Pb Geochronology and Hf Isotope of Phyllite of Langyashan Formation in Hongshuihe Iron Ore District of Eastern Kunlun and Their Geological Significance. *J. Jilin Univ. Earth Sci. Ed.* **2018**, *48*, 1085–1104. (In Chinese with English Abstract)
98. Chen, Y.X.; Pei, X.Z.; Li, R.B.; Li, Z.C.; Pei, L.; Chen, G.C.; Liu, C.J.; Li, X.B.; Yang, J. Zircon U-Pb age, geochemical characteristics and tectonic significance of metavolcanic rocks from Naij Tal Group, east section of East Kunlun. *Earth Sci. Front.* **2013**, *20*, 240–254. (In Chinese with English Abstract)
99. Li, R.B.; Pei, X.Z.; Li, Z.C. Late Silurian to Early Devonian volcanics in East Kunlun Orogen, northern Tibet Plateau: Record of post-collisional magmatism related to the Proto-Tethyan Ocean evolution. *J. Geodyn.* **2020**, *140*, 101780. [CrossRef]
100. Song, S.G.; Bi, H.Z.; Qi, S.S.; Yang, L.M.; Allen, M.B.; Niu, Y.L.; Su, L.; Li, W.F. HP-UHP Metamorphic Belt in the East Kunlun Orogen: Final Closure of the Proto-Tethys Ocean and Formation of the Pan-North-China Continent. *J. Petrol.* **2018**, *59*, 2043–2060. [CrossRef]
101. Xu, X.; Song, S.G.; Su, L. Formation age and tectonic significance of the Wanbaogou basalts in the middle East Kunlun orogenic belt. *Acta Petrol. Mineral.* **2016**, *35*, 965–980. (In Chinese with English Abstract)
102. Li, R.B.; Pei, X.Z.; Li, Z.C.; Liu, Z.Q.; Chen, G.C.; Chen, Y.X.; Wei, F.H.; Gao, J.M.; Liu, C.J.; Pei, L. Geological characteristics of Late Paleozoic-Mesozoic unconformities and their response to some significant tectonic events in eastern part of Eastern Kunlun. *Earth Sci. Front.* **2012**, *19*, 244–254. (In Chinese with English Abstract)
103. Li, R.B.; Pei, X.Z.; Li, Z.C.; Pei, L.; Chen, Y.X.; Liu, C.J.; Chen, G.C.; Liu, T.J. The depositional sequence and prototype basin for Lower Triassic Hongshuichuan Formation in the eastern segment of East Kunlun Mountains. *Geol. Bull. China* **2015**, *34*, 2302–2314. (In Chinese with English Abstract)
104. Zhang, C.F. Triassic Sedimentary Filling and Tectonic Evolution in Bayan Har Basin. Ph.D. Thesis, Northwest University, Xi'an, China, 2019. (In Chinese with English Abstract).

105. Festa, A.; Pini, G.A.; Ogata, K.; Dilek, Y. Diagnostic features and field-criteria in recognition of tectonic, sedimentary and diapiric mélanges in orogenic belts and exhumed subduction-accretion complexes. *Gondwana Res.* **2019**, *74*, 11–34. [CrossRef]
106. Liu, Z.Q.; Pei, X.Z.; Li, R.B.; Li, Z.C.; Zhang, X.F.; Liu, Z.G.; Chen, G.C.; Chen, Y.X.; Ding, S.P.; Guo, J.F. LA-ICP-MS Zircon U-Pb geochronology of the two suites of ophiolites at the Buqingshan area of the A'nyemaqen Orogenic Belt in the southern margin of East Kunlun and its tectonic implication. *Acta Geol. Sin.* **2011**, *85*, 185–194. (In Chinese with English Abstract)
107. Zhang, K.X.; Hang, J.C.; Yin, H.F.; Wang, G.C.; Wang, Y.B.; Feng, Q.L.; Tian, J. The application of radiolarians in the study of non-Smithian strata. *Sci. China Ser. D* **1999**, *29*, 542–550.
108. Hu, N.; Pei, X.Z.; Li, R.B.; Li, Z.C.; Liu, Z.Q.; Pei, L.; Liu, C.J.; Chen, Y.X.; Chen, G.C.; Yang, J. Provenance and tectonic setting study of the Maerzheng Formation at the Delistan of Buqingshan Area in the southern margin of East Kunlun. *Acta Geol. Sin.* **2013**, *87*, 1731–1747. (In Chinese with English Abstract)
109. Guo, A.L.; Zhang, G.W.; Sun, Y.G.; Zheng, J.K.; Liu, Y.; Wang, J.Q. Geochemical and spatial distribution characteristics of OIB and MORB in the A'nyemaqen Ophiolite belt: Evidence for the tectonics of the ancient oceanic ridge hot spots. *Sci. China Ser. D* **2006**, *36*, 618–629. (In Chinese with English Abstract)
110. Li, R.B.; Pei, X.Z.; Li, Z.C.; Pei, L.; Chen, G.C.; Liu, C.J.; Chen, Y.X.; Liu, Z.Q. Geochemical characteristics of Gerizhuotuo OIB and its tectonic significance in Buqingshan tectonic mélange belt, southern margin of East Kunlun Orogen. *Earth Sci. Front.* **2014**, *21*, 183–195. (In Chinese with English Abstract)
111. Isozaki, Y.; Maruyama, S.; Fukuoka, F. Accreted oceanic materials in Japan. *Tectonophysics* **1990**, *181*, 179–205. [CrossRef]
112. Safonova, I.Y.; Santosh, M. Accretionary complexes in the Asia-Pacific region: Tracing archives of ocean plate stratigraphy and tracking mantle plumes. *Gondwana Res.* **2014**, *25*, 126–158. [CrossRef]
113. Yan, Z.; Wang, Z.Q.; Fu, C.L.; Niu, M.L.; Ji, W.H.; Li, R.S.; Qi, S.S.; Mao, X.C. Characteristics and thematic geological mapping of mélanges. *Geol. Bull. China* **2018**, *37*, 167–191.
114. Santosh, M. A synopsis of recent conceptual models on supercontinent tectonics in relation to mantle dynamics, life evolution and surface environment. *J. Geodyn.* **2010**, *50*, 116–133. [CrossRef]
115. Kusky, T.M.; Windley, B.F.; Safonova, I.; Wakita, K.; Wakabayashi, J.; Polat, A.; Santosh, M. Recognition of ocean plate stratigraphy in accretionary orogens through Earth history: A record of 3.8 billion years of sea floor spreading, subduction, and accretion. *Gondwana Res.* **2013**, *24*, 501–547. [CrossRef]
116. Zhang, K.X.; He, W.D.; Xu, Y.D.; Luo, M.S.; Song, B.W.; Kou, X.H.; Zhang, Z.Y.; Xiao, Q.H.; Pan, G.T. Palaeogeographic distribution and tectonic evolution of OPS in China. *Earth Sci. Front.* **2016**, *23*, 24–30. (In Chinese with English Abstract)
117. Parkinson, I.J.; Pearce, J.A. Peridotites form the Izu-Bonin-Mariana fore-arc (ODP Leg 125): Evidence for mantle melting and melt-mantle interaction in a supra-subduction zone setting. *J. Petrol.* **1998**, *39*, 1577–1618. [CrossRef]
118. Boynton, W.V. Geochemistry of the Rare Earth Elements: Meteorite Studies. In *Rare Earth Element Geochemistry*; Henderson, P., Ed.; Elsevier: Amsterdam, The Netherlands, 1984; pp. 63–114.
119. Sun, S.S.; McDonough, W.F. Chemical and isotopic systematics of oceanic basalts: Implications for mantle composition and processed. Magmatism in Ocean Basins. *Geol. Soc. Lond. Special Public* **1989**, *42*, 313–345. [CrossRef]
120. Liu, Z.Q. Study on the Geological Characteristics and Tectonic of Buqingshan Melanges Belt, the South Margin of East Kunlun Mountains. Ph.D. Thesis, Chang'an University, Xi'an, China, 2011; pp. 1–180. (In Chinese with English Abstract)
121. Yang, J.; Pei, X.Z.; Li, R.B.; Li, Z.C.; Liu, Z.Q.; Pei, L.; Liu, C.J.; Chen, Y.X.; Chen, G.C.; Gao, J.M. Geochemical characteristics and geological implications of Haerguole basalt in Buqingshan area on the southern margin of East Kunlun Mountains. *Geol. China* **2014**, *41*, 335–350. (In Chinese with English Abstract)
122. Chen, L.; Sun, Y.; Liu, X.M.; Pei, X.Z. Geochemistry of Derni ophiolite and its tectonic significance. *Acta Petrol. Sin.* **2000**, *16*, 106–110. (In Chinese with English Abstract)
123. Chen, L.; Sun, Y.; Pei, X.Z.; Feng, T.; Zhang, G.W. Comprehensive correlation of Paleo-Tethys ophiolite and its dynamic significance: A case study of Derrni ophiolite. *Sci. China Ser. D* **2003**, *33*, 1136–1142. (In Chinese with English Abstract)
124. Yang, J.S.; Wang, X.B.; Shi, R.D.; Xu, Z.Q.; Wu, C.L. The Dur'ngoi ophiolite in East Kunlun, northern Qinghai-Tibet Plateau: A fragment of paleo-Tethyan oceanic crust. *Geol. China* **2004**, *31*, 225–239. (In Chinese with English Abstract)
125. Li, W.D.; Peng, X.P.; Kang, Z.W.; Cheng, J.F.; Zhu, Z.X.; Xu, Q.J. Petrographic geochemical features and their tectonic significance of ophiolite of Changliugou of Muztagh in East Kunlun. *Xinjiang Geol.* **2003**, *21*, 263–268. (In Chinese with English Abstract)
126. Pearce, J.A.; Norry, M.J. Petrogenetic implications of Ti, Zr, Y and Nb variations in volcanic rocks. *Contrib. Mineral. Petrol.* **1979**, *69*, 33–47. [CrossRef]
127. Yue, Y.G.; Dong, Y.P.; Sun, S.S.; He, D.F.; Hui, B.; Ren, X.; Zhang, B.; He, W.D. Mafic-ultramafic rocks in the Buqingshan Complex of the East Kunlun Orogen, northern Tibetan Plateau: Remnants of the Paleo-Tethys Ocean. *Int. Geol. Rev.* **2022**, *64*, 3149–3170. [CrossRef]
128. Wang, Y.B. The structure and evolution of the Middle Permian Seamount in Bayan Har and its adjacent area. *Sci. China Ser. D* **2005**, *35*, 1140–1149. (In Chinese with English Abstract)
129. Xu, Z.Q.; Zhao, Z.B.; Ma, X.X.; Chen, X.J.; Ma, Y. From Andean orogen to Gangdese orogeny from ocean continent subduction to continent-continent collision. *Acta Geol. Sin.* **2019**, *93*, 1–11. (In Chinese with English Abstract) [CrossRef]
130. Luo, Z.H.; Deng, J.F.; Cao, Y.Q.; Guo, Z.F.; Mo, X.X. On Late Paleozoic-Early Mesozoic volcanism and regional tectonic evolution of Eastern Kunlun, Qinghai Province. *J. Grad. Sch.* **1999**, *13*, 51–56. (In Chinese with English Abstract)

131. Garzione, C.N.; Mcquarrie, N.; Perez, N.D.; Ehlers, T.A.; Beck, S.L.; Kar, N.; Eichelberger, N.; Chapman, A.D.; Ward, K.M.; Ducea, M.N. The tectonic evolution of the Central Andean plateau and geodynamic implications for the growth of plateaus. *Annu. Rev. Earth Plant. Sci.* **2017**, *25*, 529–559. [CrossRef]
132. Defant, M.J.; Drummond, M.S.; Mount, S.T. Derivation of some modern arc magmas by melting of young subduction lithosphere. *Nature* **1990**, *347*, 662–665. [CrossRef]
133. Defant, M.J.; Drummond, M.S.; Mount, S.T. Potential example of the partial melting of the subducted lithosphere in a volcanic arc. *Geology* **1993**, *21*, 547–550. [CrossRef]
134. Whalen, J.B.; Currie, K.L.; Chappell, B.W. A-type granites: Geochemical characteristics, discrimination and petrogenesis. *Contrib. Mineral. Petrol.* **1987**, *95*, 407–419. [CrossRef]
135. Pearce, J.A.; Harris, N.B.W.; Tindle, A.G. Trace element discrimination diagrams for the tectonic interpretation of granitic rocks. *J. Petrol.* **1984**, *25*, 956–983. [CrossRef]
136. Xiong, F.H.; Meng, Y.K.; Yang, J.S.; Liu, Z.; Xu, X.Z.; Eslami, A.; Zhang, R. Geochronology and petrogenesis of the mafic dykes from the Purang ophiolite: Implications for evolution of the western Yarlung-Tsangpo suture zone, southwestern Tibet. *Geosci. Front.* **2020**, *11*, 277–292. [CrossRef]
137. Shen, H.W.; Luo, Z.H.; Mo, X.X.; Liu, C.D.; Ke, S. Underplating mechanism of Triassic granite of magma mixing origin in the East Kunlun Orogenic Belt. *Geol. China* **2005**, *32*, 386–395. (In Chinese with English Abstract)
138. Wang, K.; Wang, L.X.; Ma, C.Q.; Zhu, Y.X.; Gao, L.Y. Petrogenesis and geological implications of the Middle Triassic garnet-bearing two-mico granite from Jialuhe region, East Kunlun. *Earth Sci.* **2020**, *45*, 400–418.
139. Li, R.B. Research on the Late Paleozoic-Early Mesozoic Orogeny in East Kunlun Orogen. Ph.D. Thesis, Chang'an University, Xi'an, China, 2012; pp. 1–173. (In Chinese with English Abstract)
140. Cai, X.F.; Liu, D.M. The identification and geological significance of the lower and upper turbidite fan of the Triassic system in East Kunlun. *Mar. Geol. Lett.* **2008**, *24*, 1–32. (In Chinese with English Abstract)
141. Zhang, X.Y.; Li, W.F.; Ouyang, G.W.; Wang, C.T.; Chen, H.Q. The discovery of Early Triassic volcanic rocks in Zhanhongshan area of Qinghai Province in the eastern section of East Kunlun Mountain and its geological significance. *Geol. Bull. China* **2020**, *39*, 631–641. (In Chinese with English Abstract)
142. Cawood, P.A.; Hawkesworth, C.J.; Dhuime, B. Detrital zircon record and tectonic setting. *Geology* **2012**, *40*, 875–878. [CrossRef]
143. Pei, L.; Li, R.B.; Pei, X.Z.; Liu, J.L.; Li, Z.C.; Liu, C.J.; Chen, Y.X.; Liu, Z.Q.; Chen, G.C.; Hu, N.; et al. Sediment source analysis for the Maerzheng Formation Sandstone in Gerizhuotuo area, southern margin of East Kunlun Region: Evidence for detrital Zircon U-Pb geochronology. *Acta Geol. Sin.* **2017**, *91*, 1326–1344. (In Chinese with English Abstract)
144. Yan, Z.; Bian, Q.T.; Korchagin, O.A.; Igor, I.P.; Li, J.L.; Wang, Z.Q. Provenance of Early Triassic Hongshuichuan Formation in the southern margin of the East Kunlun Mountains: Constrains from detrital framework, heavy mineral analysis and geochemistry. *Acta Petrol. Sin.* **2008**, *24*, 1068–1078.
145. Yue, Y.G. Sedimentary Characteristic of Triassic Strata in Southern East Kunlun and the Constraints on the Closing Time of Animaqen Ocean. Master's Thesis, Northwest University, Xi'an, China, 2014. (In Chinese with English Abstract).
146. Frisch, W.; Meschede, M.; Blakey, R. *Plate Tectonics (Continental Drift and Mountain Building)*; Springer: Berlin/Heidelberg, Germany, 2011; pp. 1–197.
147. Luo, M.F. Spatial-Temporal Patter and Geological Implications of Early Paleozoic-Early Mesozoic Granitoids in the East Kunlun Orogenic Belt (Eastern Segment). Ph.D. Thesis, China University of Geosciences, Beijing, China, 2015. (In Chinese with English Abstract).
148. Xia, R. Paleotethys Orogenic Process and Gold Metallogenesis of the East Kunlun. Ph.D. Thesis, China University of Geosciences, Beijing, China, 2017. (In Chinese with English Abstract).
149. Chen, G.C.; Pei, X.Z.; Li, R.B.; Li, Z.C.; Pei, L. Geochronology and genesis of the Helegang Xilikete granitic plutons from the southern margin of the eastern East Kunlun orogenic belt and their tectonic significance. *Acta Geol. Sin.* **2013**, *87*, 1525–1541. (In Chinese with English Abstract)
150. Chung, S.L.; Liu, D.Y.; Ji, J.Q.; Chu, M.F.; Lee, H.Y.; Wen, D.J.; Lo, C.H.; Lee, T.Y.; Qian, Q.; Zhang, Q. Adakites from continental collision zones: Melting of thickened lower crust beneath southern Tibet. *Geology* **2003**, *31*, 1021–1024. [CrossRef]
151. Zhang, J.Y.; Ma, C.Q.; Xiong, F.H.; Liu, B. Petrogenesis and tectonic significance of the Late Permian-Middle Triassic calc-alkaline granites in the Balong region, eastern Kunlun Orogen, China. *Geol. Mag.* **2012**, *149*, 892–908. [CrossRef]
152. Gao, Y.B.; Li, W.Y.; Qian, B.; Li, K.; Li, D.S.; He, S.Y.; Zhang, Z.W.; Zhang, J.W. Geochronology, geochemistry and Hf isotopic compositions of the granitic rocks related with iron mineralization in Yemaquan deposit, East Kunlun, NW China. *Acta Petrol. Sin.* **2014**, *30*, 1647–1665. (In Chinese with English Abstract)
153. Pan, T. Classification of metallogenic units in Qinghai, China. *J. Earth Sci. Environ.* **2017**, *39*, 16–33. (In Chinese with English Abstract)
154. Stampfli, G.M. Tethyan oceans. In *Tectonics and Magmatism in Turkey and the Surrounding Area*; Bozkurt, E., Winchester, J.A., Piper, J.D.A., Eds.; Geological Society, Special Publications: London, UK, 2000; Volume 173, pp. 1–23.
155. Stampfli, G.M.; Borel, G.D. A plate tectonic model for the Paleozoic and Mesozoic constrained by dynamic plate boundaries and restored synthetic oceanic isochrons. *Earth Planet Sci. Lett.* **2002**, *196*, 17–33. [CrossRef]
156. Stampfli, G.M.; Hochar, C.; Vérard, C.; Wilhem, C.; vonRaumer, J. The formation of Pangea. *Tectonophysics* **2013**, *593*, 1–19. [CrossRef]

157. Wang, Y.; Qian, X.; Cawood, P.A.; Liu, H.; Feng, Q.; Zhao, G.; Zhang, Y.; He, H.; Zhang, P. Closure of the East Paleotethyan Ocean and amalgamation of the Eastern Cimmerian and Southeast Asia continental fragments. *Earth-Sci. Rev.* **2018**, *186*, 195–230. [CrossRef]
158. Li, C. A review on 20 Years' Study of the Longmu Co-Shuanghu-Lancang River Suture Zone in Qinghai-Xizang (Tibet) Plateau. *Geol. Rev.* **2008**, *54*, 105–119. (In Chinese with English Abstract)
159. Zhai, Q.G.; Jahn, B.M.; Wang, J.; Su, L.; Mo, X.X.; Wang, K.L.; Tang, S.H.; Lee, H.Y. The Carboniferous ophiolite in the middle of the Qiangtang terrane, Northern Tibet: SHRIMP U-Pb dating, geochemical and Sr-Nd-Hf isotopic characteristics. *Lithos* **2013**, *168*, 186–199. [CrossRef]
160. Zhai, Q.G.; Jahn, B.M.; Wang, J.; Hu, P.Y.; Chung, S.L.; Lee, H.Y.; Tang, S.H.; Tang, Y. Oldest Paleo-Tethyan ophiolitic mélange in the Tibetan Plateau. *Geol. Soc. Am. Bull.* **2016**, *128*, 355–373. [CrossRef]
161. Moghadam, H.S.; Stern, R.J. Ophiolites of Iran: Keys to understanding the tectonic evolution of SW Asia: (I) Paleozoic ophiolites. *J. Asian Earth Sci.* **2014**, *4*, 8.
162. Moghadam, H.S.; Stern, R.J. Ophiolites of Iran: Keys to understanding the tectonic evolution of SW Asia: (II) Mesozoic ophiolites. *J. Asian Earth Sci.* **2014**, *12*, 16. [CrossRef]
163. Xiao, W. Accretionary Tectonics of the Western Kunlun Orogen, China: A Paleozoic-Early Mesozoic, Long-Lived Active Continental Margin with Implications for the Growth of Southern Eurasia. *J. Geol.* **2005**, *113*, 687–705. [CrossRef]
164. Metcalfe, I. Gondwana dispersion and Asian accretion: Tectonic and Paleogeographic evolution of eastern Tethys. *J. Asian Earth Sci.* **2013**, *66*, 1–33. [CrossRef]
165. Metcalfe, I. Tectonic evolution of the Malay Peninsula. *Asian Earth Sci.* **2013**, *76*, 195–213. [CrossRef]
166. Dickinson, W.R. Interpreting Provenance Relations from Detrital Modes of Sandstones. In *Provenance of Arenites*; Zuffa, G.G., Ed.; D. Reidel Publishing Company: Dordrecht, The Netherlands, 1985; Volume 148, pp. 333–361.
167. Roger, F.; Jolivet, M.; Malavieille, J. The tectonic evolution of the Songpan-Garzê (North Tibet) and adjacent areas from Proterozoic to Present: A synthesis. *J. Asian Earth Sci.* **2010**, *39*, 254–269. [CrossRef]
168. Yang, T.N.; Hou, Z.Q.; Wang, Y.; Zhang, H.R.; Wang, Z.L. Late Paleozoic to Early Mesozoic tectonic evolution of northeast Tibet: Evidence from the Triassic composite western Jinsha-Garzê-Litang suture. *Tectonics* **2012**, *31*, TC4004. [CrossRef]
169. Tan, J.; Wei, J.H.; Zhao, X.F.; Zhao, S.Q.; Liu, Y.; Zhang, F.; Liu, X.Y. Late Paleozoic to early Mesozoic Paleo-Tethys tectonic evolution of central NE Tibetan Plateau: Insights from the Zhiduo mafic-ultramafic complex. *Lithos* **2020**, *364–365*, 105534. [CrossRef]
170. Ding, Q.F.; Jiang, S.Y.; Sun, F.Y. Zircon U-Pb geochronology, geochemical and Sr-Nd-Hf isotopic compositions of the Triassic granite and diorite dikes from the Wulonggou mining area in the Eastern Kunlun Orogen, NW China: Petrogenesis and tectonic implications. *Lithos* **2014**, *205*, 266–283. [CrossRef]
171. Liu, J.L.; Sun, F.Y.; Li, L.; Zhao, F.F.; Wang, Y.D.; Wang, S.; Zhang, Y.T. Geochronology, geochemistry and Hf isotopes of Gerizhuotuo complex intrusion in west of Animaqen Suture Zone. *Earth Sci.* **2015**, *40*, 965–981. (In Chinese with English Abstract)
172. Ferrari, O.M.; Hochard, C.; Stampfli, G.M. An alternative plate tectonic model for the Paleozoic-Early Mesozoic Paleotethyan evolution of Southeast Asia (Northern Thailand-Burma). *Tectonophysics* **2008**, *451*, 346–365. [CrossRef]
173. Ma, C.Q.; Xiong, F.H.; Zhang, J.Y.; Liu, B.; Huang, J.; Jiang, H.A. Effects of magmatism from plate subduction to post-orogenic stage: Evidence for Early Permian-Late Triassic mafic dykes in East Kunlun Mountains. *Acta Geol. Sin.* **2013**, *87*, 79–81. (In Chinese with English Abstract)
174. Ma, C.Q.; Xiong, F.H.; Yin, S.; Wang, L.X.; Gao, K. Intensity and cyclicity of orogenic magmatism: An example from a Paleo-Tethyan granitoid batholith, Eastern Kunlun, northern Tibetan Plateau. *Acta Petrol. Sin.* **2015**, *31*, 3555–3568. (In Chinese with English Abstract)
175. Paterson, S.R.; Ducea, M.N. Arc magmatic tempos: Gathering the evidence. *Elements* **2015**, *11*, 91–97. [CrossRef]
176. Zhou, H.; Zhang, D.; Wei, J.; Wang, D.; Santosh, M.; Shi, W.; Chen, J.; Zhao, X. Petrogenesis of Late Triassic mafic enclaves and host granodiorite in the Eastern Kunlun Orogenic Belt, China: Implications for the reworking of juvenile crust by delamination-induced asthenosphere upwelling. *Gondwana Res.* **2020**, *84*, 52–70. [CrossRef]
177. Wang, G.C.; Xiang, S.; Wang, A.; Garver, J.; Wintsch, R.; Zhang, K.X. Thermochronological constraint to the processes of the East Kunlun and adjacent areas in Mesozoic-Early Cenozoic. *Earth Sci.-J. China Univ. Geosci.* **2007**, *32*, 605–614. (In Chinese with English Abstract)
178. Chen, X.H.; McRivette, M.W.; Li, L.; Yin, A.; Jiang, R.B.; Wan, J.L.; Li, H.J. Thermochronological evidence for multi-phase uplifting of the East Kunlun Mountains, northern Tibetan Plateau. *Geol. Bull. China* **2011**, *30*, 1647–1660. (In Chinese with English Abstract)
179. Yuan, W.M.; Zhang, A.K.; Tian, C.S.; Feng, X.; Hao, N.N.; Feng, Y.L.; Chen, X.Q. The tectonic events in Halongxiuma district, East Kunlun Mountains, Qinghai-Tibet Plateau: Evidence from fission track thermochronology. *Radiat. Measur.* **2019**, *123*, 63–68. [CrossRef]
180. Tian, P.; Yuan, W.; Yang, X.; Feng, Z.; Chen, X.; Yuan, E. Multi-stage tectonic events of the Eastern Kunlun Mountains, Northern Tibetan Plateau constrained by fission track thermochronology. *J. Asian Earth Sci.* **2020**, *198*, 104–428. [CrossRef]
181. Feng, K.; Li, R.B.; Pei, X.Z.; Li, Z.C.; Liu, C.J.; Pei, L. Zircon U-Pb Chronology, Geochemistry and Geological Significance of Late Triassic Intermediate-Acid Volcanic Rocks in Boluositai Area, East Kunlun Orogenic Belt. *Earth Sci.* **2022**, *47*, 1194–1216.
182. Feng, K.; Li, R.B.; Pei, X.Z.; Li, Z.C. Dating and geochemical characteristics of Dagele granite in the eastern margin of East Kunlun orogenic belt, China and their tectonic implications. *J. Earth Sci. Environ.* **2020**, *42*, 442–463.

183. Li, Z.C.; Pei, X.Z.; Bons, P.D.; Li, R.B.; Pei, L. Petrogenesis and tectonic setting of the early middle Triassic subduction-related granite in the eastern segment of East Kunlun: Evidences from petrology, geochemistry, and zircon U-Pb-Hf isotopes. *Int. Geol. Rev.* **2021**, *64*, 698–721. [CrossRef]
184. Guo, Z.Z.; Jia, Q.Z.; Li, Y.Z.; Li, J.C. Zircon U-Pb geochronology and geochemical characteristics of the Reshui monzogranites in the eastern Kunlun and their tectonic significances. *Bull. Mineral. Petrol. Geochem.* **2016**, *35*, 1318–1328.
185. Wu, Z.N.; Ji, W.H.; He, S.P.; Chen, S.J. LA-ICP-MS zircon U-Pb dating and geochemical characteristics of granodiorite in Rilonggou area, Xinghai County, Qinghai Province. *Geol. Bull. China* **2015**, *34*, 1677–1688.
186. Kong, H.L.; Li, J.C.; Jia, Y.Z.; Jia, Q.Z. LA-ICP-MS zircon U-Pb dating and its geological implications of the tonalite from Xiaoyuanshan iron-polymetallic ore district in Qimantag Mountain, Qinghai Province. *Geol. Sci. Technol. Inf.* **2016**, *35*, 8–16.
187. Qian, B.; Gao, Y.B.; Li, K.; Zhang, Z.W. Zircon U-Pb-Hf isotopes and whole rock geochemistry constraints on the petrogenesis of iron-rare metal mineralization related alkaline granitic intrusive rock in Yugouzi area, eastern Kunlun, Xinjiang. *Acta Petrol. Sin.* **2015**, *31*, 2508–2520.
188. Zhang, M.Y.; Feng, C.Y.; Wang, H.; Li, D.X. Petrogenesis and tectonic implications of the Late Triassic syenogranite in Qimantag area, East Kunlun Mountains. *Acta Petrol. Min.* **2018**, *37*, 197–210.
189. Liu, J.N.; Feng, C.Y.; He, S.Y.; Pei, R.F.; Li, D.X. Zircon U-Pb and Phlogopite Ar-Ar Ages of the Monzogranite from Yemaquan Iron-zinc Deposit in Qinghai Province. *Geotecton. Metallog.* **2017**, *12*, 1158–1170.
190. Yang, T.; Li, Z.M.; Zhang, L.; Song, Z.B. Geological and Geochemical Characteristics of the Tawenchahanxi Granites in East Kunlun and Its Tectonic Significance. *Geol. J. China Univ.* **2017**, *23*, 452–464.
191. Qu, H.Y.; Feng, C.Y.; Pei, R.F.; He, S.Y. Thermochronology of Hutouya Skarn-type Copper-Lead-Zinc polymentallic ore district in the Qimantage area, Qinghai Province. *Acta Geol. Sin.* **2015**, *89*, 498–509.
192. Yan, W.; Qiu, D.M.; Ding, Q.F. Geochronology, petrogenesis, source and Its structural significance of Houtougou Monzogranite of Wulonggou area in Eastern Kunlun Orogen. *J. Jinlin Univ.* **2016**, *46*, 443–460.